KUOPION YLIOPISTON JULKAISUJA C. LUONNONTIETEET JA YMPÄRISTÖTIETEET 268
KUOPIO UNIVERSITY PUBLICATIONS C. NATURAL AND ENVIRONMENTAL SCIENCES 268

ERNA KALEVA

Optimization of Quantitative High-Frequency Ultrasound Imaging of Articular Cartilage

Doctoral dissertation

To be presented by permission of the Faculty of Natural and Environmental Sciences of the University of Kuopio for public examination in Auditorium L22, Snellmania building, University of Kuopio, on Friday 11th December 2009, at 12 noon

Department of Physics, University of Kuopio
Department of Clinical Neurophysiology,
Kuopio University Hospital and University of Kuopio
Department of Clinical Physiology and Nuclear Medicine,
Kuopio University Hospital and University of Kuopio

KUOPION YLIOPISTO

KUOPIO 2009

Distributor: Kuopio University Library
P.O. Box 1627
FI-70211 KUOPIO
FINLAND
Tel. +358 40 355 3430
Fax +358 17 163 410
http://www.uku.fi/kirjasto/julkaisutoiminta/julkmyyn.shtml

Series Editor: Professor Pertti Pasanen, Ph.D.
Department of Environmental Science

Author's address: Department of Physics
University of Kuopio
P.O. Box 1627
FI-70211 KUOPIO
FINLAND
Tel. +358 50 375 0781
Fax +358 17 162 585
E-mail: erna.kaleva@uef.f

Supervisors: Professor Jukka Jurvelin, Ph.D.
Department of Physics
University of Kuopio

Professor Juha Töyräs, Ph.D.
Department of Physics
University of Kuopio

Adjunct Professor Simo Saarakkala, Ph.D.
Department of Physics
University of Kuopio

Reviewers: Research Scientist Amena Saïed, Ph.D.
Laboratoire d'Imagerie Paramétrique
CNRS - Univesité Pierre et Marie Curie, France

Professor Georg N. Duda, Ph.D.
Julius Wolff Institut
Charité - Universitätsmedizin Berlin, Germany

Opponent: Principal Research Scientist Jun-Kyo Francis Suh, Ph.D.
Convergence Technology Laboratories
Korea Institute of Science and Technology, Korea

ISBN 978-951-27-1406-3
ISBN 978-951-27-1461-2 (PDF)
ISSN 1235-0486

Kopijyvä
Kuopio 2009
Finland

Kaleva, Erna. Optimization of quantitative high-frequency ultrasound imaging of articular cartilage. Kuopio University Publications C. Natural and Environmental Sciences 268. 2009. 77 p.
ISBN 978-951-27-1406-3
ISBN 978-951-27-1461-2 (PDF)
ISSN 1235-0486

ABSTRACT

Osteoarthrosis (OA) is a common musculoskeletal disease affecting the quality of life especially amongst the elderly. In OA, the cartilage tissue in articulating joints, such as the knee, degenerates and eventually wears out, exposing the subchondral bone. The first symptoms of OA - pain and limited mobility - usually appear during the late stage of the disease, when the changes in the cartilage are already irreversible. Early signs of OA cannot be detected with the current clinical imaging methods.

Quantitative high-frequency ultrasound imaging is a promising method for detecting early degenerative changes in articular cartilage. This thesis work has further developed the quantitative ultrasound methodology for the assessment of cartilage in order to improve the sensitivity of OA diagnostics. Bovine and human osteochondral samples were studied *in vitro*. The acoustic parameters associated with ultrasound reflection from the surface of the cartilage and roughness of the superficial cartilage were evaluated. The values of the acoustic parameters were related with the structural integrity of the cartilage as assessed by microscopical imaging and histological scoring. Acoustic parameters defined in time and frequency domains or using wavelet transform were compared with each other in order to find the optimal parameter for detecting the changes related to OA. The effects of ultrasound frequency, temporal sampling frequency, spatial sampling step and angle of incidence of the ultrasound pulse with respect to the articular surface were investigated to optimize the imaging parameters and to clarify the effect of sources of uncertainties associated with potential clinical measurements. For the first time, a sample-specific acoustic model was constructed to numerically evaluate the effects of varying surface roughness, material parameters and inclination of the articular surface on the ultrasound reflection.

The wavelet parameters, including both the time and frequency information of the original reflected ultrasound signal, were not superior to the traditional time or frequency domain parameters. On the contrary, their complexity might well hinder their usability in a clinical measurement. The acoustically determined roughness of the cartilage surface was the most reliable indicator of the degeneration of the tissue. The major limitation to the use of the roughness parameter is the greater technical requirements demanded of the imaging system in comparison to those needed with the parameters describing the amplitude of the reflected ultrasound. In particular, the ultrasound transducer must be focused and the frequency should be high (> 5 MHz). The strong attenuation of the high-frequency ultrasound hinders the simultaneous assessment of the subchondral bone, which is also affected in OA. However, the roughness parameter was less susceptible to the angle of incidence of the ultrasound pulse with respect to the surface of the cartilage. The modeling results supported the findings of the present experimental studies and indicated that ultrasound successfully detects changes in the cartilage that are characteristic of OA.

In conclusion, the presented methods provide useful information about the optimization of quantitative high-frequency ultrasound imaging of articular cartilage, and may be utilized in further development of clinical ultrasound applications.

PACS Classification: 43.35.+d
Universal Decimal Classification: 534.321.9
National Library of Medicine Classification: QT 34, QT 36, WE 300, WE 348, WN 208
Medical Subject Headings: Musculoskeletal Diseases/diagnosis; Joint Diseases/diagnosis; Osteoarthritis/diagnosis; Cartilage, Articular/ultrasonography; Collagen; Proteoglycans; Diagnostic Imaging; Ultrasonography; Ultrasonics; Acoustics; Surface Properties

To Tuomas

ACKNOWLEDGMENTS

This study was carried out during the years 2006-2009 at the Department of Physics, University of Kuopio, at the Department of Clinical Neurophysiology, Kuopio University Hospital and University of Kuopio and at the Department of Clinical Physiology and Nuclear Medicine, Kuopio University Hospital and University of Kuopio.

I am grateful to professor Jukka Jurvelin, Ph.D., my main supervisor and the leader of our research group Biophysics of Bone and Cartilage, BBC, for giving me the opportunity to work in this successful and inspiring group.

I thank my second supervisor professor Juha Töyräs, Ph.D. for guiding my thesis work and always finding the time for enthusiastically solving scientific challenges.

I wish to express my gratitude also to my third supervisor, adjunct professor Simo Saarakkala, Ph.D., for his valuable hands-on help and maintaining a considerate attitude throughout the thesis process.

I am grateful to the official reviewers of this thesis, Research Scientist Amena Saïed, Ph.D. and Univ.-Prof. Dr. Georg N. Duda, Ph.D., for their constructive criticism and encouraging comments. I thank Professor Ewen Macdonald, D.Pharm. for linguistic review.

Working in the ever growing BBC research group has been a real joy during the last years. The openness and friendly atmosphere have helped me through some tough phases during the thesis project.

Particularly, I wish to thank Eveliina Lammentausta, Heikki Nieminen, and Mikko Nissi for "showing me the ropes" in the beginning, Pauno Lötjönen and Antti Aula for assistance in sample preparation, Matti Timonen for programming custom made measurement software when needed, Janne Karjalainen for introducing me the principles of ultrasonic measurements, Tuomas Virén for participating in the exhausting nocturnal measurement sessions, Tuomo Silvast for conducting the microCT measurements of my samples and Jukka Liukkonen for his efforts in modeling.

My thanks go also to the past and present members and visitors of the BBC group and Rami Korhonen's research group who I have had the priviledge of working with (in alphabetical order): Jatta Berberat, Mikko Hakulinen, Yale Huang, Hanna Isaksson, Petro Julkunen, Panu Kiviranta, Yevgeniya Kobrina, Harri Kokkonen, Rami Korhonen, Katariina Kulmala, Mikko Laasanen, Markus Malo, Juho Marjanen, Mika Mikkola, Mika Mononen, Jaana Mäkitalo, Laetitia Nasser, Viktoria Prantner, Sarianne Pääkkö, Ossi Riekkinen, Lassi Rieppo, Lauri Rytkönen, Elli-Noora Salo, Dimitry Semenov, Petri Tanska, Mikael Turunen, Siru Turunen, Cora Verheijen and Sami Väänänen.

I want to acknowledge the staff at the Institute of Biomedicine, Anatomy and the BioMater Centre, especially Eija Rahunen, Kari Kotikumpu, Riikka Kärnä, Mikko Lammi, Heikki Helminen, Virpi Miettinen, Arto Koistinen and Ritva Sormunen for their efforts and help in sample processing and related issues.

I also wish to thank the staff at the Department of Physics and especially Jarkko Leskinen for degassing bucketloads of saline for my measurements.

I acknowledge Atria Suomi Oy, Kuopio, Finland for providing bovine joints as research material.

This thesis work was financially supported by several Finnish institutions: Kuopio University Hospital (EVO grants 5041719 and 5031337), the National Graduate

School of Musculoskeletal Disorders and Biomaterials (TBGS) and Päivikki and Sakari Sohlberg Foundation (grant 49720) (and my mother). The North Savo Regional Fund of the Finnish Cultural Foundation, Jenny and Antti Wihuri Foundation and I-SKTS, Foundation for Advanced Technology of Eastern Finland are acknowledged for their highly valuable personal grants.

I send my dearest thanks to the friends and relatives who have believed in me and given my life a deeper meaning. Especially I want to thank my parents Heli and Jouni Kaleva and my brother Sampo Kaleva for supporting me on the path I have chosen. I also cordially thank Pepsi, Ensio, Purre and Unto for their soft, unconditional support.

I owe my deepest gratitude to my significant other Tuomas for his endless love and support, occasional technical and liguistic assistance and bearing the side effects during the years of my thesis work.

Kuopio, November 22nd, 2009

Erna Kaleva

ABBREVIATIONS

1D	one-dimensional
2D	two-dimensional
3D	three-dimensional
A/D	analog/digital
A-mode	1D amplitude representation of a reflected ultrasound wave
B-scan	2D ultrasound image
CCD	charge-coupled device
CT	computed tomography
EDTA	ethylenediaminetetraacetate acid
FDTD	finite difference time domain
FEPA	Federation of European Producers of Abrasives
FFT	fast Fourier transform
FMC	femoral medial condyle
FT	femoral trochlea
FWHM	full width at half of the maximum
FWTM	full width at one tenth of the maximum
LPG	lateral patellar groove
MRI	magnetic resonance imaging
MTP	medial tibial plateau
OA	osteoarthrosis, osteoarthritis
PAT	patella
PBS	phosphate-buffered saline
PG	proteoglycan
QUI	quantitative ultrasound imaging
RMS	root mean square
ROC	receiver operating characteristic
SEM	scanning electron microscopy
US	ultrasound
WT	wavelet transform
X-ray	radiographic imaging

SYMBOLS AND NOTATIONS

a	dilation parameter or scale
A	amplitude of the ultrasound signal
A_{i}	amplitude of the i:th A-mode US signal
$A_{\mathrm{i}}^{\mathrm{ref}}$	amplitude of the reference A-mode US signal
$A_0(z, f)$	frequency and depth-dependent attenuation function in PBS
α	ultrasound attenuation coefficient
b	location parameter
c	speed of sound, ultrasound wave velocity
CV	coefficient of variation
CQI	cartilage quality index
d	distance
d_{i}	distance between US transducer and sample in i:th A-mode US signal
D	diameter of ultrasound transducer
D_{beam}	cross-sectional diameter of ultrasound beam
Δf	frequency bandwidth
E	Young's (elastic) modulus
$E(f)$	acoustoelectric transfer function
ED	echo duration
f	frequency of ultrasound or pseudo frequency
f_c	central frequency of a mother wavelet function
F	focal length
F_z	focal zone
ϕ	bulk viscosity
$G(f)$	acquisition system transfer function
$H_{\mathrm{s}}^2(z, f)$	surface-integrated diffraction function in pulse echo mode
η	shear viscosity
I	intensity of the ultrasound signal
IRC	integrated reflection coefficient
IRC_{exp}	experimental integrated reflection coefficient
IRC_{model}	modeled integrated reflection coefficient
j	imaginary unit
k	wave number
λ	wavelength or first Lamé constant
m	number of A-mode ultrasound signals or power
mM	molarity, millimoles per liter
MM	maximum magnitude
μ	second Lamé constant
n	number of samples or datapoints
ν	Poisson's ratio
ω	angular temporal frequency
p	statistical significance

r	correlation coefficient
R	ultrasound reflection coefficient
$R(f)$	frequency-dependent reflection coefficient
$R_{\text{ref}}(f)$	frequency-dependent reflection coefficient of the reference signal
$R^{\text{dB}}(f)$	frequency-dependent reflection coefficient in decibels
ρ	density
$S(z, f)$	frequency spectrum of the ultrasound reflection signal from the cartilage surface
$S_{\text{ref}}(z, f)$	frequency spectrum of the ultrasound reflection signal from the reference surface
T	transmission coefficient
SD	standard deviation
t	time
$T(a, b)$	continuous wavelet transform coefficient
θ_i	angle of incidence
θ_r	angle of refraction
TOF	time of flight
u	particle displacement
URI	ultrasound reflection index
v_{l}	longitudinal ultrasound wave velocity
$\boldsymbol{w}$	2D displacement vector
x	1D signal
ψ	mother wavelet function
z	distance or depth
z_{R}	Rayleigh distance
Z	acoustic impedance
$\langle \cdots \rangle$	spatial average
$\lvert \cdots \rvert$	absolute value
∂	partial difference operator
∇	gradient operator
$\nabla \cdot$	divergence operator
$*$	complex conjugate

LIST OF ORIGINAL PUBLICATIONS

This thesis is based on the following original articles referred to in the text by their Roman numerals:

I Kaleva E., Saarakkala S., Töyräs J., Nieminen H.J. and Jurvelin J.S.: In vitro comparison of time-domain, frequency-domain and wavelet ultrasound parameters in diagnostics of cartilage degeneration, *Ultrasound in Medicine and Biology*, 34(1):155-9 (2008);
doi:10.1016/j.ultrasmedbio.2007.06.028

II Kaleva E., Saarakkala S., Jurvelin J.S., Virén T. and Töyräs J.: Effects of ultrasound beam angle and surface roughness on the quantitative ultrasound parameters of articular cartilage, *Ultrasound in Medicine and Biology*, 35(8):1344-1351 (2009);
doi:10.1016/j.ultrasmedbio.2009.03.009

III Kaleva E., Töyräs J., Jurvelin J.S., Virén T. and Saarakkala S.: Effects of ultrasound frequency, temporal sampling frequency and spatial sampling step on the quantitative ultrasound parameters of articular cartilage, *IEEE Trans Ultrason Ferroelectr Freq Control*, 56(7):1383-1393 (2009);
doi:10.1109/TUFFC.2009.1194

IV Kaleva E., Liukkonen J., Töyräs J., Saarakkala S., Kiviranta P. and Jurvelin J.S.: Two-dimensional finite difference time domain model of ultrasound reflection from normal and osteoarthritic human articular cartilage surface, accepted for publication in *IEEE Trans Ultrason Ferroelectr Freq Control* (2009).

The thesis also contains previously unpublished data.

CHAPTER I
Introduction

Osteoarthrosis (OA), also referred to as osteoarthritis, is a very common musculoskeletal disease of the joints. Typically it is initiated by injuries, exessive loading, obesity and aging [18, 103, 106]. In addition to the decrease in the individual's quality of life, OA causes significant costs to the society because of lost working ability and treatment expenses [18, 35, 45, 86, 87, 130]. In the USA, the number of people with clinical OA has gone up from 21 million in 1995 to 27 million in 2008 [86], and the medical and prescription costs per patient alone were more than one thousand dollars yearly [35]. Aging of the population will further increase the socio-economical impact of OA in Finland also.

Progressive OA is associated with an increase of the water content, depletion of the proteoglycans (PG) and disruption of the collagen matrix in cartilage [6, 17, 101, 105]. If an intervention is to be made while the osteoarthritic changes might still be reversible, one would need to have a method capable of detecting early changes in the cartilage, such as fibrillation of the surface. Further, the possibility to monitor and reliably quantify properties of healing cartilage is a prerequisite for developing and improving remedies and surgical repair methods. The resolution of the current clinical imaging methods (X-ray imaging, magnetic resonance imaging) is not sufficient to detect the earliest signs of degeneration of the cartilage [77]. The qualitative arthroscopic examination, based on the visual assessment of the surface of the cartilage, is subjective and unable to detect early degeneration of the tissue [116, 115].

High frequency ultrasound has been shown to reveal spontaneous and enzymatically or mechanically induced morphological changes in articular cartilage both in human and animal *in vitro* studies [2, 24, 25, 26, 29, 52, 65, 93, 111, 122, 131, 133, 134, 135, 137, 144]. Furthermore, quantitative ultrasound imaging (QUI) has been used for evaluation of healing of cartilage lesions after surgical repair both spontaneously [81, 85] and with tissue-engineered cartilage [55, 56]. Quantitative ultrasound parameters defined in time and frequency domains have been applied successfully for diagnosing the integrity of articular cartilage *in vitro* [25, 133]. Attempts have been made to define parameters based on the wavelet transform (WT) of an ultrasound signal as a way of estimating surface irregularity and thickness of articular cartilage [52]. The WT analysis has been applied also *in vivo* during examination of human knee, ankle, elbow and wrist cartilage during arthroscopic surgery [51, 54, 112, 136].

In study I of this thesis, time-domain, frequency-domain and WT ultrasound parameters were evaluated to determine their potential for detecting degenerative chan-

ges in the surface of articular cartilage. The usefulness of the WT parameters was compared with that of the time and frequency domain parameters. It was hypothesized that because of the intrinsic ability of the WT analysis to simultaneously preserve the time-domain and frequency-domain information of an ultrasound signal, it might provide more useful information about the cartilage tissue than the time- or frequency-domain analyses separately.

Non-perpendicular angle of incidence of the ultrasound beam or the natural curvature of the articular surface can jeopardize the reliability of the QUI measurements. In material sciences, the reflection and scattering of ultrasound from inclined planar rough phantoms have been studied [121, 154]. Although the dependence of specular reflection on the inclination of an interface is generally well understood for homogeneous materials, this is not the case with biological materials, *e.g.* the ultrasound reflected and scattered from a degenerated articular surface. The susceptibility of the QUI of cartilage to variations in the angle of incidence of the ultrasound beam relative to the investigated surface has not been studied thoroughly. However, it is known that the angle of incidence of the ultrasound beam on the cartilage can affect the amplitude of the reflected ultrasound differently in healthy and degenerated cartilage [13, 24]. In study II, the susceptibility of the ultrasound parameters to non-perpendicularity of the ultrasound angle of incidence with respect to the articular surface was investigated. Visually intact and degenerated cartilage surfaces were included in the study to investigate the effect of the surface characteristics on the angular dependence of the parameters.

In OA, subchondral sclerosis and osteophyte formation are known to occur in parallel with the cartilage degeneration [18]. Therefore, the ultrasonic analysis of the subchondral bone could provide diagnostically valuable information. Encouraging results have been achieved in simultaneous ultrasound diagnostics of the cartilage and the subchondral bone; the shape of the frequency profiles [13] or the ratio of the reflection coefficients of the cartilage and bone at 10 MHz [14] have been found to differentiate degraded cartilage from normal tissue. Changes in acoustic impedances, reflecting the changes in the elastic properties and density of cartilage and subchondral bone, have indicated subchondral sclerosis at 50 MHz [90]. The amplitude of the reflection from the cartilage-bone interface has been found to increase in spontaneously degenerated tissue [133]. Unfortunately, excessive attenuation at high (> 10 MHz) ultrasound frequencies limits the imaging depth and can prevent effective ultrasonic imaging of the subchodral bone. For example, the measurement of the ultrasound scattering from within the bone becomes unfeasible. Therefore, in bone diagnostics, low ($\sim$5 MHz) ultrasound frequencies are generally used [20, 44, 47, 58, 70]. However, low ($\sim$ 5 MHz) ultrasound frequencies have not been applied in the QUI of the cartilage. Furthermore, the frequency and focusing affect the ultrasound beam diameter and thus the imaging resolution of the ultrasound method. Similarly, the size of the spatial sampling step and temporal sampling frequency were hypothesized to affect the quantitative ultrasound parameters - especially the ultrasound roughness index (*URI*) which was introduced earlier as a way of conducting ultrasonic determination of surface roughness of cartilage [131]. Different sampling steps and temporal sampling frequencies have been used in QUI studies of articular cartilage [25, 131, 133], but their effects on the calculated parameters have not been studied thoroughly previously. Study III aimed to clarify to what extent the focusing and frequency of the

ultrasound beam, temporal sampling frequency and the size of the spatial sampling step could affect the reliability of the ultrasound parameters. Furthermore, the applicability of the low-frequency ultrasound, frequently used in the assessment of bone, was investigated for evaluating the integrity of the surface of the articular cartilage.

Experiments have revealed that the roughness of the surface [2, 13, 24, 131] and the collagen content [144] of the cartilage affect the ultrasound reflection from the articular surface. Generally, it is known that the density of a material also affects the ultrasound reflection [151]. In OA, all these factors change concurrently [17], and thus evaluating the effects of changes in any individual factor experimentally is difficult. A numerical model could enable the evaluation of the contributions of these factors separately. However, ultrasound reflection from the surface of the cartilage has not, to our knowledge, been numerically modeled before. In study IV, for the first time, a sample-specific finite difference time domain (FDTD) model was developed for ultrasonic measurements of articular cartilage in pulse-echo geometry. The modeling results were compared with results from experimental measurements of the same samples with an identical geometry. Contributions of the roughness of the surface and the material parameters of the cartilage to the ultrasound reflection were evaluated. Furthermore, the effects of a non-perpendicular angle of incidence of the ultrasound beam were modeled.

In summary, this thesis work is a systematic experimental and numerical investigation of technical factors affecting the ultrasonic evaluation of integrity of articular cartilage.

CHAPTER II

Articular cartilage

2.1 Structure and composition

Articular cartilage is aneural and avascular connective tissue that covers the epiphyses of articulating bones [17]. Articular cartilage distributes loads and creates, together with synovial fluid, an almost frictionless interface between the bones. The thickness of the tissue varies, depending on the location, age, weight, gender and species [8, 34, 48, 102, 139]; in the human knee joint, the thickness of the cartilage is typically between 1 and 6 mm [8, 34, 48].

Interstitial water makes up about 65 - 80 % of the total mass of the cartilage [16, 17]. The solid part of the cartilage tissue consists mainly of a type II collagen fibril network embodying interfibrillar proteoglycan (PG) macromolecules and chondrocytes [16, 17].

The structure of the articular cartilage is highly anisotropic and inhomogeneous (figure 2.1). In the superficial zone, the collagen fibrils are thin (diameter $\approx$ 20 - 50 nm [50]) and aligned with the surface of the cartilage. In the transitional zone, the fibrils start gradually to thicken (reaching a diameter of 200 - 300 nm [50]) and bend towards the subchondral bone, and reach a perpendicular orientation in the deep zone. The collagen fibrils penetrate into the subchondral bone via the calcified cartilage layer. The collagen content of fully hydrated cartilage tissue is lowest in the disorganized transitional zone and higher in the organized deep and superficial zones [16, 50, 105].

The collagen matrix is maintained under tension by the osmotic pressure attributable to the negatively charged proteoglycans [30, 97]. The proteoglycans bind chemically to the collagen fibers or become mechanically entrapped within the collagen matrix [16]. The concentration of the PGs increases as a function of the depth in the cartilage. Since the interstitial water fills the molecular framework, the water content conversely decreases as a function of the depth [16].

The chondrocyte, which is responsible for the cartilage matrix synthesis, is the only cell type within normal articular cartilage [16]. In human cartilage tissue, the chondrocytes make up only about 1 % of the total volume of the cartilage tissue [16]. The shape of the chondrocytes changes from flat in the superficial zone to being more spherical in the deep zone. The density of the chondrocytes decreases as a function of the depth in the cartilage [50]. The outermost thin layer of cartilage, on top of the superficial layer, is, however, cell-free [17]. This dense web of collagen fibrils forms a

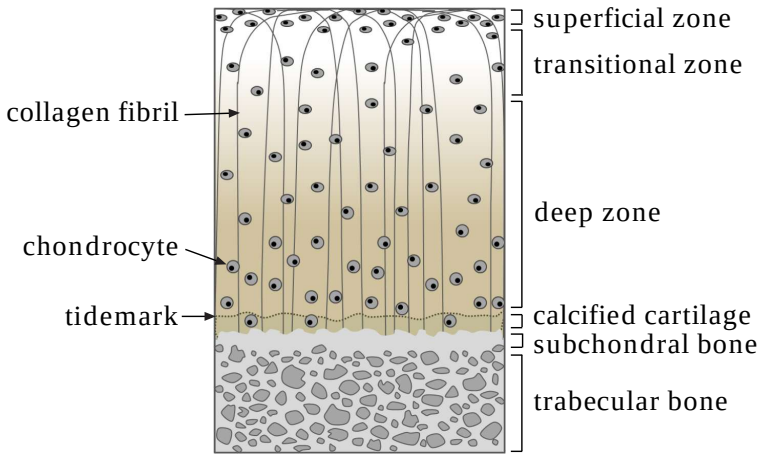

Figure 2.1: The structure of articular cartilage tissue.

"skin" of the articular cartilage that prevents leakage of PGs out of the cartilage and antibodies and proteins into the cartilage [16].

2.2 Function

Articular cartilage provides a low-friction interface between the articulating bones. Intact cartilage surface is very smooth, showing roughness values less than 1 μm [39, 60]. The coefficient of friction between lubricated cartilage surfaces can be as low as 0.01 [22, 38, 99]. In comparison, a Teflon-Teflon interface has a coefficient of friction of about 0.04. The low friction between the articulating surfaces can be explained by two lubrication mechanisms. During dynamic loading (*e.g.* jumping) the interstitial fluid is pressurized and thus it supports the load and diminishes the friction [7]. During static loading (*e.g.* standing), the surface of cartilage is lubricated by synovial macromolecules, *e.g.* lubricin [42, 64].

Another important function of the articular cartilage is to transmit and distribute forces between the articulating bones and to protect the bones from excessive loads [16, 105]. The articular cartilage is a poroviscoelastic material that has an excellent ability to adapt to various types of loads. The behavior of the cartilage under loading is highly dependent on the type of the loading. When there is a short impulse load, such as during walking or running, the interstitial fluid does not have time to squeeze out of the cartilage because the permeability of the tissue to fluid flow is normally quite low (4.7×10^{-15} m^4/Ns [105]). The collagen matrix resists the deformation pressure caused by the nearly incompressible interstitial water thus making the cartilage very stiff under impact loading [76, 105]. The superficial collagen fibers are also responsible for the tensile stiffness and resistance to shear forces on the superficial cartilage [72, 80]. In situations of static long-term loading, such as standing, the

role of the proteoglycans becomes more important [84]. With time, the fluid flows out ot the tissue until a static equilibrium, primarily due to the electrostatic repulsion between the PGs, is reached [105]. The equilibrium modulus of cartilage is in the range of 0.2 - 0.6 MPa as opposed to the instant modulus, which can be in the range of 1 - 16 MPa [84]. The Poisson's ratio ν for healthy cartilage is in the range of 0.05 - 0.4 [50, 84].

2.3 Osteoarthrosis; pathophysiology, diagnosis and treatment

Osteoarthrosis is a severe degenerative joint disease typically found in the knee, hand, hip and spine [4, 17]. The cause of primary osteoarthrosis (OA) is poorly understood, but its prevalence is strongly associated with aging [10, 17]. Sometimes OA can be initiated by injuries or else it can be a hereditary, inflammatory, developmental, metabolic or neurologic disorder, and in that case is referred to as secondary OA [17]. The disease is, however, primarily characterized by disruption of the structure and impairment of the functional properties of the articular cartilage, together with increased subchondral bone remodeling [17, 138]. Failure of the chondrocytes to repair or stabilize the cartilage tissue leads to the final stage of OA.

Increase in the water content of cartilage [17, 96, 98], depletion of proteoglycans in superficial cartilage [101, 105] and degradation of collagen network [101] are known to occur at an early stage of OA. These compositional and structural changes make cartilage softer and more prone to further damage [6]. Disruption of the collagen network, in contrast to depletion of proteoglycans, is especially harmful because it is regarded as a virtually irreversible process [16, 40, 146].

The earliest visually detectable sign of OA is fibrillation of the cartilage surface. In advanced OA, the roughness of degenerated cartilage may be over 100 μm [104], which is visually detectable. It is especially important to be able to evaluate the changes in the properties of the superficial layer of the articular cartilage because the mechanical properties of the tissue are highly dependent on the integrity of the superficial collagen matrix [68, 80, 129, 149]. Furthermore, degradation of the superficial collagen matrix can cause leakage of the superficial PGs out of the cartilage tissue and, thus, further affect the equilibrium stiffness of the cartilage [129]. In the final stage of OA, the wear and tear on the cartilage can be excessive, and the subchondral bone may be revealed [12, 17, 150]. In addition, the degenerative changes in the cartilage, structural and biomechanical changes of the subchondral bone, such as formation of osteophytes and cysts or subchondral sclerosis, are also known to occur in even the early stages of OA [5, 11, 17, 28, 127].

It is common that only the first symptoms, *e.g.* joint stiffness, limited range of motion or pain associated with joint motion, convince the patients to make their way to clinical examinations [4, 17]. By that time, a significant portion of the cartilage tissue may be already worn out and at this advanced stage of OA, the cartilage will not be able to recover. The current diagnosis techniques of OA include X-ray imaging, magnetic resonance imaging (MRI) and arthroscopy. With X-ray imaging, only an indirect indication of cartilage wear, *i.e.* the narrowing of the joint space, is revealed. The increased density of subchondral bone and osteophytes can also be detected with radiography, but as well as the joint space narrowing, these are typically signs of advanced OA. The MRI enables visualization of the cartilage tissue as well. Unfortunately, the

resolution of the clinical MRI is not sufficient to allow the detection of the incipient fibrillation of the tissue. Arthroscopy enables direct inspection of the surface of the articular cartilage, but the evaluation is based only on qualitative visual evaluation and mechanical palpation. All in all, the current diagnosis methods are unable to detect with any degree of accuracy the early OA changes, such as initial fibrillation of the superficial articular cartilage.

Since the ability of cartilage to repair itself is limited, an early diagnosis of cartilage degeneration is of critical importance in order to initiate preventive, even reconstructive actions. Elimination or reduction of certain risk factors, such as obesity, muscle weakness and repetitive and intense loading of the joint, is possible, whereas others, such as genetical background, gender or aging, cannot be influenced. The pain associated with OA can be relieved with analgesics and anti-inflammatory drugs [4, 17] and the mobility of the joint is claimed to be improved with intra-articular hyluronan injection [118].

Currently, there is no cure for the primary OA, but disease modifying osteoarthritis drugs, such as glycosamine sulfate [63] and calcitonin [71], are under constant research and development. However, the effectiveness of the glycosamine sulfate treatment is controversial [100, 125]. Surgical methods, such as mosaicplasty or autologous chondrocyte transplantation have been developed for repair of focal cartilage defects caused by injuries [15]. In some cases, the results have been good [17], but the long term durability of the repaired tissue is questionable [32, 78].

Further development of the existing and new drugs and surgical methods for OA require a sensitive method capable of imaging and quantifying the effectiveness of the treatments [126]. The current clinical methods lack sufficient sensitivity to detect the changes related to early OA, whereas quantitative ultrasound imaging (QUI) has shown potential *e.g.* in detecting the incipient fibrillation of the articular surface. The QUI, however, is not yet a clinically applicable method. This thesis work has focused on mapping the techical limitations and optimizing the imaging parameters of the QUI method as a way of advancing the potential clinical applications of ultrasound.

CHAPTER III

Ultrasonic assessment of articular cartilage

3.1 Basic physics of ultrasound

Ultrasound is a mechanical wave motion, the frequency of which is beyond the human hearing range, *i.e.* above 20 kHz. Ultrasound can be generated through the piezoelectric phenomenon (Greek: piezo ≈ press or squeeze), where the electrical signal from a pulser is converted into mechanical vibration in the piezoelectric material of the ultrasound transducer. The particles in a medium can vibrate along or across the direction of the propagating ultrasound wave. When the direction of the vibration of the particles and the propagation of the wave is the same, the rarefaction and compression fronts in the medium form a longitudinal wave. When the oscillation of the particles happens perpendicular to the direction of the wave propagation, a transverse, *i.e.* shear wave is formed. Non-viscous fluids do not support shear waves [151]. In articular cartilage, the shear waves are negligible in comparison to the longitudinal waves [41, 94].

The linear wave equation describing simple harmonic vibration, derived from Newton's second law, can be used to approximate for the vibration caused by ultrasound in a homogeneous, linear and isotropic material (equations (3.1) and (3.2) in table 3.1). When ultrasound propagates in and between media, the main physical interactions are attenuation, reflection and refraction. The angles, θ, of reflection and refraction between two materials obey Snell's law (equation (3.3) in table 3.1). The reflection and refraction (equations (3.4) and (3.5) in table 3.1) are governed by the differences in acoustic impedances Z (equation (3.6) in table 3.1) of the media [151].

In reality, the interaction between ultrasound and a medium is never completely lossless because of different attenuation mechanisms. The intensity I_z of ultrasound propagating in direction z in a medium attenuates through both absorption and scattering (equation (3.7) in table 3.1). The absorption coefficient $\alpha_{\text{absorption}}$ (equation (3.8) in table 3.1) depends on the properties of the material, and for soft tissues, such as articular cartilage, the power of the frequency dependence, m, is 0.8-1.2 in a frequency range from 100 kHz to 10 MHz [152, 119]. The attenuation is usually expressed as a ratio $\alpha_{\text{absorption}}/f$ and for soft tissues one attains a range of 0.3 - 3.5 dB cm^{-1} MHz^{-1} in the frequency range from 100 kHz to 10 MHz [151, 152, 155]. Absorption mechanisms involving conversion of energy from the vibrational form include *e.g.* elastic hysteresis, viscosity and heat conduction in fluids [151]. In biological materials, such

Table 3.1: Basic equations for physics of ultrasound

Parameter/law	Equation	Number
Linear wave equation	$\frac{\partial^2 u}{\partial z^2} - \frac{1}{c^2}\frac{\partial^2 u}{\partial t^2} = 0$	(3.1)
Wave function	$u(z,t) = u_0 e^{j(\omega t - kz)}$	(3.2)
Snell's law	$\frac{\sin\theta_i}{\sin\theta_r} = \frac{c_1}{c_2}$	(3.3)
Reflection coefficient	$R = \frac{p_{\text{reflected}}}{p_{\text{incident}}} = \frac{Z_2\cos\theta_{\text{incident}} - Z_1\cos\theta_{\text{reflected}}}{Z_2\cos\theta_{\text{incident}} + Z_1\cos\theta_{\text{reflected}}}$	(3.4)
Transmission coefficient	$T = \frac{p_{\text{transmitted}}}{p_{\text{incident}}} = \frac{2Z_2\cos\theta_{\text{incident}}}{Z_2\cos\theta_{\text{incident}} + Z_1\cos\theta_{\text{reflected}}}$	(3.5)
Acoustic impedance	$Z = \rho c$	(3.6)
Intensity of ultrasound propagating in z-direction	$I_z = I_0 e^{-2(\alpha_{\text{absorption}} + \alpha_{\text{scattering}})z}$	(3.7)
Attenuation coefficient in biological tissues	$\alpha_{\text{absorption}} = \alpha_0 f^m$, $m \approx 0.8$ - 1.2	(3.8)

α_0 = attenuation coefficient
$c = \frac{f}{\lambda}$ = velocity of the ultrasound wave in the direction of the ultrasound propagation
f = frequency of ultrasound
j = imaginary unit
$k = 2\pi/\lambda$ = wave number
λ = wavelength of ultrasound
$\omega = 2\pi f$ = angular frequency
ρ = density
t = time
θ_i = angle of incidence
θ_r = angle of refraction
u = the displacement amplitude of a particle in the medium where ultrasound propagates
u_0 = the displacement amplitude of a particle in the medium where ultrasound propagates at $t = 0$
z = direction of the ultrasound propagation

as articular cartilage, relaxation originating from molecular or lattice vibrational energy or translational energy is the dominant absorption interaction [151]. Scattering of ultrasound is caused by elastic discontinuities within the medium. The nature of scattering is determined by the size and shape of the scatterers. If the size of the scatterers is much smaller than the wavelength of the ultrasound, Rayleigh scattering occurs and the ultrasound is scattered uniformly in all directions. When the size of the scatterers is close to the wavelength, the distribution of the scattered ultrasound depends strongly on the acoustic impedance and the geometry of the scatterers and the scattering distributions can be very complex. When the size of the scatterers becomes much larger than the wavelength, the proportion of scattering diminishes and the specular reflection becomes the dominant interaction [151].

3.2 Technical aspects of ultrasound imaging

In this thesis, the ultrasonic measurements were done in a pulse-echo geometry, with the same transducer being used to transmit and receive the ultrasonic signal, because the articular surface was the target of interest. Ultrasonic detection of details in the micrometer scale, such as fibrillation of the superficial articular cartilage, poses demanding requirements for the resolution of the ultrasound transducer.

The axial resolution of an ultrasound system is defined as the ability to resolve two reflectors in parallel to the direction of the ultrasound beam axis and thus it is directly related to the wavelength of the ultrasound [31]. As a general rule, the wavelength of an ultrasound pulse decreases as the frequency of the ultrasound increases. However, the attenuation of ultrasound also increases as a function of the frequency (see equa-

tion (3.8) in table 3.1) and thus there is a limit to the resolution that can be achieved by increasing the frequency [49].

When pulsed ultrasound is used, the axial resolution, roughly determined as half of the spatial pulse length, is better than with continuous ultrasound. Further, the frequency spectrum of the ultrasonic pulse widens as the duration of the pulse shortens. Thus, with shorter pulses, *e.g.* the attenuation of the ultrasound can be determined within a wider range of frequencies.

The ultrasound field, generated by a piezoelectric transducer, can be roughly divided into two zones: the near field or Fresnel zone and the far field or Fraunhofer zone. In the near field, the ultrasound pulse fluctuates between high-amplitude maxima and minima due to diffraction [37]. The distance from the surface of the transducer to the last maximum of the near field, where the characteristic focus of the transducer occurs, is called the Rayleigh distance, z_{R}.

$$z_{\mathrm{R}} = \frac{\pi D^2}{4\lambda}\,, \tag{3.9}$$

where D is the diameter of a circular transducer element. Beyond the Rayleigh distance, the far field begins and the pressure of the ultrasound signal gradually drops to zero. For pulsed ultrasound, the pressure fluctuation in the near field is not as significant as for continuous ultrasound. Thus, with pulsed ultrasound, measurements can be conducted in the near field as well.

The lateral resolution of the ultrasound system is primarily determined by the diameter of the ultrasound beam at the region of interest. The smaller the beam diameter, the better the lateral resolution and also the greater the energy reflected back from an acoustic interface. Usually, the beam diameter is defined by using the -6 dB limit, where the intensity of the beam has dropped to half of the maximum in the direction perpendicular to the beam axis:

$$D_{\mathrm{beam}}(-6\mathrm{dB}) \approx 1.028\frac{Fc}{fD} \approx 0.257\, D\frac{F}{z_{\mathrm{R}}}\,, \tag{3.10}$$

where F is the focal length, *i.e.* the distance from the surface of the transducer to the location of the maximum amplitude in the ultrasound field [128]. For an unfocused transducer, equation (3.10) can be used by setting the fraction $F/z_{\mathrm{R}} = 1$.

To increase the lateral resolution, ultrasound transducers can be focused *e.g.* by using lenses, reflectors, concave transducers or electrical control of phase differences of the ultrasound waves transmitted by an array of transducers. The focal zone F_z, can be defined as the distance around the focus along the beam direction, where the intensity of the beam is within -6 dB of the maximum:

$$F_z = \frac{2F^2}{z_{\mathrm{R}} + \frac{F}{2}}\,. \tag{3.11}$$

In the experimental ultrasonic measurements, as a means to maximize the signal-to-noise ratio, the region of interest should always be within the focal zone.

For planar surfaces, the amplitude of the ultrasound echo signal recorded at normal incidence decreases as the roughness of the surface increases [121, 154]. Furthermore, when the angle of incidence of the ultrasound beam increases, the energy of the received signal decreases [154]. When ultrasound is used to assess a rough curved or

tilted surface in a pulse-echo geometry, a focused transducer should be used. This can help to minimize the effects of the radius of curvature or the non-perpendicular angle of incidence *e.g.* on roughness discrimination [23, 154]. When the angle of incidence is sufficiently large, the incoherent scattering dominates and the roughness effects become more evident [23]. These issues have to be considered carefully, when naturally contoured articular surfaces with variable degenerative states are being assessed with ultrasound.

3.3 Quantitative ultrasonic evaluation of articular cartilage

Articular cartilage is a poroviscoelastic, inhomogenous and anisotropic material, the acoustic properties of which depend on the composition and structure of the tissue.

The speed of sound in cartilage depends on the anatomical location and integrity of the tissue [82, 143]. Maturation has also been reported to affect the speed of sound in rat and porcine cartilage [26, 62, 73]. A reduced collagen content reduces the speed of sound [65, 122, 143]. The collagen fibril orientation also affects the speed of ultrasound; the speed is highest when the orientation of the fibrils lies parallel to the direction of the ultrasound beam [43, 89, 120]. A decrease in the PG content [65, 123, 143, 144, 156] or an increase in the water content [123, 143] also leads to reduced speed of sound. Typically the values of speed of ultrasound in normal human or bovine cartilage of the knee joint are in the range 1580 - 1760 m/s [65, 91, 107, 109, 110, 111, 120, 143, 144]. In enzymatically or spontaneously degenerated cartilage, the speed of sound is slightly decreased to 1550 - 1660 m/s [65, 107, 109, 111, 144].

The density of cartilage has been measured to be about 1050 kg/m^3 [67]. When the water content of damaged cartilage increases, the density approaches the density of water, 1000 kg/m^3. Assuming isotropy and elasticity, the characteristic acoustic impedance of the cartilage can be estimated from its density and the speed of sound. Based on the above values, the acoustic impedance of human or bovine cartilage would thus fall between 1.55 - 1.85 $\times 10^6$ kg/(m^{2}s). However, the acoustic impedance of human articular cartilage has been discovered to increase continuously from the surface towards the subchondral bone, and a mean value of $(2.12 \pm 0.02) \times 10^6$ kg/(m^{2}s) determined with 50 MHz ultrasound has been reported [90]. The characteristic acoustic impedance of water is about 1.52 $\times 10^6$ kg/(m^{2}s) [153] and according to equation (3.4), the ultrasound reflection coefficient at a water - cartilage interface can be assumed to vary between 1% and 10%. This has been confirmed experimentally also (see table 3.2).

The attenuation of ultrasound depends strongly on the frequency of the ultrasound [92, 151]. The attenuation of ultrasound in cartilage has been found to correlate significantly with the histologic integrity of the tissue [109]. An increase in the attenuation coefficient has been related to PG loss [65] and breaking of the intermolecular cross-links in collagen [3]. Nieminen *et al.* reported integrated attenuation coefficient for bovine articular cartilage to be 2.65 $\pm$ 0.58 dB/mm at 10 MHz [109] and Senzig *et al.* reported 3.2 - 7.5 Np/cm ($\approx$ 2.78 - 6.51 dB/mm) at 10 - 40 MHz [135]. The absorption of shear waves in soft tissues is much greater than that of longitudinal waves [41, 94], and thus for practical purposes the shear waves can usually be neglected.

Ultrasound reflection and scattering from the surface and backscattering from the internal cartilage are extremely complex processes [33, 66, 153]. The ultrasound reflec-

tion parameters are able to distinguish osteoarthritic changes [25], maturation [25], enzymatical degradation [131] and spontaneously repaired cartilage [85] from intact cartilage. Enzymatically induced PG depletion has been detected with ultrasound by recording an echo from the digestion front [144, 148]. However, the collagen content is the dominant component determining the acoustic impedance and hence the reflection properties of cartilage [36, 124, 144]. Reflected ultrasonic signals have been used to differentiate PG-depleted or collagen meshwork-disrupted cartilage from normal tissue based on changes in the features of their frequency spectra [13]. Quantitatively, the ultrasound reflection and scattering from the surface of the cartilage have been evaluated and correlated with the roughness and composition of the cartilage *in vitro* [2, 24, 25, 52, 82, 85, 131, 133]. Quantitative ultrasonic evaluation of human articular cartilage has been tested also *in vivo* during arthroscopic surgery [53, 54, 112, 136]. Recently, a potentially less invasive method utilizing intravascular ultrasound probes has been tested for evaluation of articular cartilage as well [61, 147].

The roughening of the cartilage surface has been quantified using the ultrasound roughness index, *URI* [82, 131], the degree of broadening in the angle-dependent pressure amplitude [2], incoherent mean backscattered power [24] as well as the integrated reflection coefficient *IRC* [25] and reflection coefficient *R* [85]. Histological scoring of the structure of the cartilage has been successfully related with the semi-quantitative ultrasonographic grading [29, 88, 137]. Ultrasonic measurements have also been combined with mechanical compression *e.g.* in elastography [117, 79], indentation [83, 140, 159] and water-jet indentation [158].

Some values presented in the literature for the surface reflection parameters *R* and *IRC* and the roughness parameter *URI* are listed in table 3.2.

Table 3.2: Ultrasonically determined values of reflection coefficient *R*, integrated reflection coefficient *IRC* and ultrasound roughness index *URI* for the surface of articular cartilage.

Species	Site	*n*	Treatment/status		*R*(%)	*IRC* (dB)	*URI* (μm)	*f*(MHz)	Study
bovine	PAT	8	emery paper P60	before	4.4 ± 1.5	-28.0 ± 3.4	7.7 ± 1.6	20	[131]
				after	2.2 ± 0.6	-32.6 ± 2.0	28.8 ± 15.1		
		6	emery paper P120	before	3.8 ± 1.2	-29.0 ± 2.4	7.3 ± 1.9		
				after	1.8 ± 0.4	-33.6 ± 1.6	18.4 ± 3.1		
		6	emery paper P240	before	3.8 ± 1.0	-28.3 ± 2.0	6.8 ± 1.1		
				after	2.5 ± 0.6	-31.0 ± 1.5	12.4 ± 2.8		
		6	emery paper P360	before	3.6 ± 1.2	-28.1 ± 2.2	8.5 ± 1.8		
				after	2.4 ± 0.7	-31.3 ± 3.0	13.3 ± 3.9		
		6	collagenase	before	2.9 ± 1.2	-30.9 ± 3.1	10.6 ± 3.0		
				after	0.4 ± 0.1	-46.9 ± 2.5	34.8 ± 11.8		
		6	trypsin	before	4.2 ± 0.8	-27.8 ± 2.2	7.2 ± 1.5		
				after	3.7 ± 0.6	-28.3 ± 1.2	9.0 ± 2.4		
		6	chondroitinase ABC	before	3.8 ± 2.0	-30.0 ± 4.2	12.3 ± 8.0		
				after	4.2 ± 2.7	-29.6 ± 5.1	12.5 ± 4.5		
bovine	PAT	11	intact		5.3 ± 0.9	-26.7 ± 1.6	7.4 ± 1.2	20	[133]
		21	degenerated		2.4 ± 1.6	-34.1 ± 5.5	24.2 ± 15.5		
bovine	FMC	6	healthy		2.7	-30.2	12.0	20	[82]
	LPG	6			2.5	-31.2	14.5		
	MTP	6			1.5	-33.6	15.5		
	PAT	12			4.7	-27.0	8.0		
porcine	FT	5	control		6.2	-	7.5	20	[85]
		8	lesion		1.6	-	44.0		
		8	adjacent to lesion		4.4	-	10.0		
bovine	PAT	6	control	0 h	2.80 ± 0.22	-	-	29.4	[111]
				6 h	2.77 ± 0.24	-	-		
		6	collagenase	0 h	2.43 ± 0.76	-	-		
				6 h	0.52 ± 0.21	-	-		
		6	trypsin	0 h	2.14 ± 0.82	-	-		
				4 h	1.91 ± 0.87	-	-		
rat	PAT	8	control (placebo)	1 week	-	-23.2	-	50	[25]
		8		2 weeks	-	-22.9	-		
		8		3 weeks	-	-21.4	-		
		8		4 weeks	-	-23.1	-		
		8	mono-iodo-acetic acid	1 week	-	-26.4	-		
		8		2 weeks	-	-27.9	-		
		8		3 weeks	-	-29.8	-		
		8		4 weeks	-	-	-		
		2	non-injected	1 week	-	-22.4	-		
		2		2 weeks	-	-22.0	-		
		2		3 weeks	-	-22.3	-		
		2		4 weeks	-	-22.1	-		
rat	PAT	8	immature	control	-	-22.9	-	55	[123]
		8		degenerater	-	-23.3	-		
		8	mature	control	-	-20.9	-		
		8		degenerated	-	-20.6	-		
rat	PAT	12	control	5 d	-	-21.1	-	55	[62]
		12		14 d	-	-20.6	-		
		12		21 d	-	-21.1	-		
		12	ZYM	5 d	-	-25.6	-		
		12		14 d	-	-23.9	-		
		12		21 d	-	-24.9	-		
		12	NPX	5 d	-	-24.8	-		
		12		14 d	-	-26.1	-		
		12		21 d	-	-22.0	-		
		12	DEX	5 d	-	-22.2	-		
		12		14 d	-	-20.0	-		
		12		21 d	-	-20.1	-		

The values of *R*, *IRC* and *URI* without error limits have been estimated from column charts. All used ultrasound transducers were focused.
PAT = patella
FMC = femoral medial condyle
LPG = lateral patellar groove
MTP = medial tibial plateau
FT = femoral trochlea
ZYM = zymosan
NPX = naproxen
DEX = dexamethasone

CHAPTER IV

Aims of the present study

This thesis work has continued earlier research on the ultrasonic assessment of articular cartilage and further investigated the ultrasound methodology for quantitative evaluation of osteoarthrotic changes in the cartilage. Acoustic parameters describing changes occurring at an early stage of osteoarthrosis were determined and compared with histological reference data and data acquired from a sample-specific numerical model.

The specific aims of this thesis were:

1. to compare quantitative time domain, frequency domain and wavelet transform ultrasound parameters to determine their diagnostic potential in evaluating degenerative changes of surface of articular cartilage
2. to clarify whether the ultrasound roughness index (*URI*) is less susceptible to variations in the angle of incidence of the ultrasound beam than the corresponding reflection and scattering parameters
3. to specify the optimal characteristics and operation settings of an ultrasound transducer for evaluation of superficial articular cartilage
4. to develop a sample-specific finite difference time domain (FDTD) model for ultrasonic measurements of articular cartilage in a pulse-echo geometry and evaluate the effects of roughness of the articular surface and angle of incidence of the ultrasound beam on the ultrasound reflection and scattering from the cartilage surface.

CHAPTER V

Materials and methods

This thesis consists of four independent studies (I-IV). For studies I and IV, the ultrasound raw data and histological sections have been extracted from earlier studies (Saarakkala *et al.* [133] and Kiviranta *et al.* [75]). In studies I and IV, the raw data has been analyzed from a different perspective. For studies II and III, all sample material was new. The materials and methods used in each study are summarized in table 5.1

Table 5.1: Summary of materials and methods used in studies I - IV. All measurements were conducted in room temperature (typically 20 - 23 °C)

Study	Samples	n	Methods	Parameters
I	Bovine patellae		Ultrasound imaging	*R*, *IRC*, *URI*,
	* visually intact	11		*MM*, *ED*
	* spontaneously degenerated	21	Histological analysis	Mankin score, CQI
II	Bovine patellae		Ultrasound imaging	*R*, *IRC*, *URI*
	* visually intact	8	Light microscopy	RMS roughness
	* mechanically degraded	6	Histological analysis	Mankin score
	Human tibiae		Scanning electron microscopy	qualitative
	* spontaneously fibrillated	1		
	* spontaneously PG-depleted	1		
III	Bovine patellae		Ultrasound imaging	*R*, *IRC*, *URI*,
	* visually intact	8		*MM*, *ED*,
	* mechanically degraded	8	Light microscopy	RMS roughness
	Human tibiae		Histological analysis	Mankin score
	* spontaneously fibrillated	1	Scanning electron microscopy	qualitative
	* spontaneously PG-depleted	1		
	Phantoms			
	* P60 (mean particle size 269 μm)	1		
	* P120 (mean particle size 125 μm)	1		
	* P240 (mean particle size 58.5 μm)	1		
	* P360 (mean particle size 40.5 μm)	1		
IV	Human patellae		Ultrasound imaging	IRC_{exp}
	* healthy	24	FDTD-modeling	IRC_{model}
	* early degeneration	11	Light microscopy	RMS roughness
	* advanced degeneration	8		

CQI = cartilage quality index
ED = echo duration
FDTD = finite difference time domain
IRC = integrated reflection coefficient
IRC_{exp} = experimentally determined *IRC*
IRC_{model} = modeled *IRC*
MM = maximum magnitude
n = number of the samples
PG = proteoglycan
R = reflection coefficient
RMS = root mean square
URI = ultrasound roughness index

5.1 Articular cartilage samples

Osteochondral samples from bovine patellae and human patellae and tibiae were used in this thesis work. The bovine knees were obtained from the local abattoir (Atria Oyj, Kuopio, Finland) and opened within a few hours *post mortem*. Human cadaver knees were obtained from Jyväskylä Central Hospital, Jyväskylä, Finland, as approved by the national authority (National Authority for Medicolegal Affairs, Helsinki, Finland, permission 1781/32/200/01). The human patellae and proximal epiphyses of tibiae were detached from cadavers at autopsy within 48 h *post mortem*, wrapped in gauze damped with phosphate buffered saline (PBS) and frozen until subsequent sample preparation.

The bovine samples used in study I were originally prepared for an earlier study [132]. In that study, cylindrical osteochondral plugs (diameter = 19 mm) were taken from the upper quadrants of the patellae. Cartilage surfaces with both normal and degenerated appearances were included in the study. For studies II and III, cylindrical osteochondral plugs were prepared from visually intact lateral upper quadrants of the bovine patellae (diameter = 6 mm) and lateral plateaus of the human tibiae (diameter = 4 mm). The data for the human samples used in study IV were extracted from an earlier study [75]. In that study, 14 patellae were collected from right knees. The measurements were conducted *in situ* from six sites on the patellae: superomedial, superolateral, central medial, central lateral, inferomedial and inferolateral.

After the preparation, all the samples were stored in PBS in a freezer and thawed at room temperature just before the measurements. During the measurements, the samples were immersed in PBS containing inhibitors of proteolytic enzymes (5 mM ethylenediaminetetraacetic acid (EDTA) and 5 mM benzamide HCl). In studies II and III, some of the bovine samples were degraded mechanically to simulate fibrillation of the cartilage surface typical of OA. The cartilage surfaces were ground along two perpendicular directions with emery paper (P120, FEPA standard; average particle diameter = 125 μm) just before the measurements.

5.2 Phantoms

For study III, five phantoms (area = 1 cm^2) with different surface roughnesses were made. Emery paper (FEPA standard: P360, P240, P120 or P60) or a polished steel plate was pressed on the surface of hot-setting adhesive (3M Jet-melt, 3764-Q; 3M, St. Paul, USA). The average particle sizes of the emery papers were 40.5 μm (P360), 58.5 μm (P240), 125 μm (P120) and 269 μm (P60). Since the adhesive material was homogeneous, only one acoustic interface was formed between the PBS and the phantom during the ultrasonic measurements.

5.3 Ultrasonic imaging and quantitative measurements

The properties of the ultrasound transducers used in this thesis are listed in table 5.2. The principles of the measurement systems are described next and the measurement geometries are illustrated in figures 5.1, 5.2 and 5.3.

Table 5.2: Summary of the characteristics of the ultrasound transducers used in this thesis.

Transducer model (Panametrics)	V3758M	V3193	V307	XMS310
Nominal central frequency (MHz)	20	50	5	10
Measured -6 dB frequency range (MHz)	6 - 28	8.0 - 41.5	2.7 - 6.3	9.0 - 14.5
Focal length (mm)	15.01	25.0	49.9	-
Focal zone (mm)	3	3.7	8.8	-
Element diameter (mm)	6.35	6.35	25.4	2.0
Confocal beam diameter (μm)	200	120	600	-
Study	I	II & III	III	III & IV

5.3.1 Dermascan

The data for study I was measured with a Dermascan 20 MHz ultrasound instrument (Cortex Ltd., Hadsund, Denmark) (see table 5.2) [133]. An external data-acquisition system (Physical Acoustics Corporation, Princeton, NJ, USA) operating at a sampling frequency of 250 MHz was used. The A-mode reflections from the cartilage surface were recorded using spatial sampling steps of 76 μm. The maximum reflection amplitude was used as an indicator while manually adjusting the cartilage surface perpendicularly in respect to the direction of the ultrasound beam [133]. Details of the measurement are presented in an earlier study [133] and the principle of the measurement is visualized in figure 5.1.

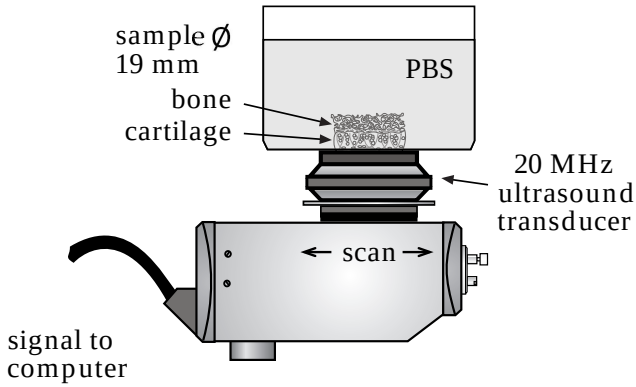

Figure 5.1: Schematic presentation of the measurement geometry of study I. Not to scale.

5.3.2 UltraPAC

The UltraPAC scanning acoustic system (Physical Acoustics Corporation, Princeton, NJ, USA) consists of a 0.5 to 100 MHz ultrasound pulser-receiver board and a 500 MHz 8-bit A/D board. The 3D motor system enables moving the ultrasound transducer in 5.1 μm steps in the XY-plane and in 3.8 μm steps in the Z-direction. The

UltraPAC system was used with 50 MHz (studies II and III), 10 MHz (study III) and 5 MHz (study III) ultrasound transducers (see table 5.2). The whole cartilage surfaces of the osteochondral samples were imaged with 20 μm spatial steps and a sampling frequency of 500 MHz. In study II, the surfaces of the samples were tilted 2°, 5° or 7° using goniometers. The principle of the measurements is visualized in figure 5.2.

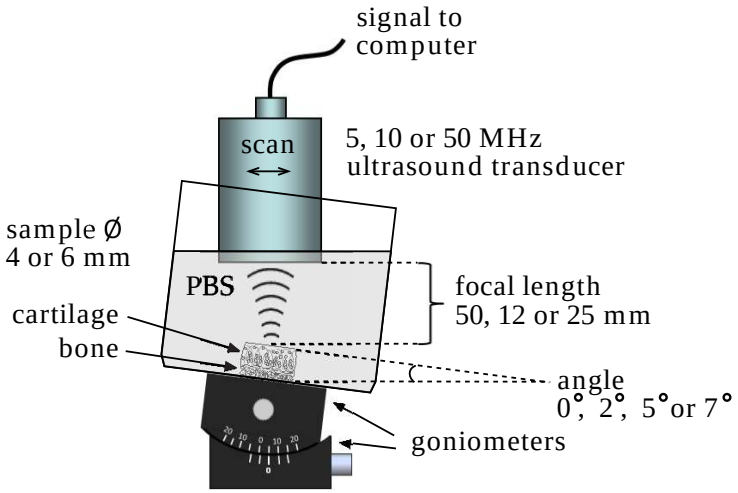

Figure 5.2: Schematic presentation of the measurement geometry applid in studies II and III. Not to scale.

5.3.3 Ultrascan

The UltraScan device combines a hand-held arthroscopic indentation instrument (Artscan200, Artscan Oy, Helsinki, Finland) with a miniature 10 MHz-ultrasound transducer (Panametrics XMS310, Panametrics Inc., Waltham, MA, USA) (see table 5.2) [83]. The ultrasound reflections from cartilage surface were recorded at a constant distance (3 mm) at six measurement sites on human patellae (see figure 5.3) with the UltraScan device by Kiviranta *et al.* [75]. In study IV of this thesis, the ultrasound raw data was analyzed from a different perspective and compared with sample-specific finite difference modeling results.

5.4 Quantitative ultrasound parameters

The ultrasonic analyses in this thesis (see table 5.1) were conducted with LabVIEW (v. 6.1, National Instruments, Austin, TX, USA) (in study I) and MATLAB (v. 6.0-7.5.0, The Mathworks Inc. Natick, MA, USA) (in studies I-IV) sotfwares.

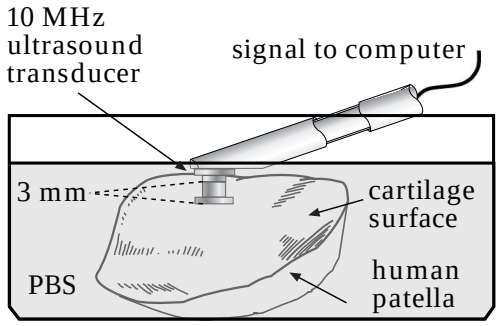

Figure 5.3: Schematic presentation of the measurement geometry applied in study IV. Not to scale.

5.4.1 Reflection parameters *IRC* and *R*

The amplitude of the ultrasound signal reflected from the surface of the cartilage or phantom was quantified with the integrated reflection coefficient *IRC* (dB) in frequency domain [25] and the reflection coefficient *R* (%) in time domain [131]. The reflection amplitude from the cartilage or phantom surface was normalized with the reflection amplitude from a perfect reflector at the same distance. In studies II and III, the reference reflection was recorded from PBS-polished steel interface and in studies I and IV from the PBS-air interface. According to equation (3.4) (on page 26), about 94% of the ultrasound pressure is reflected from the PBS-steel interface and about 99% from the PBS-air interface.

In order to calculate the *IRC*, the frequency spectra for the cartilage surface $S(z, f)$ and for the reference signal $S_{\text{ref}}(z, f)$ at depth z at normal incidence need to be determined. $S_{\text{ref}}(z, f)$ can be determined as

$$S(z, f) = E(f) \times G(f) \times A_0(z, f) \times H_{\text{s}}^2(z, f) \times R(f)\,, \tag{5.1}$$

where $E(f)$ is the acoustoelectric transfer function, $G(f)$ is the acquisition system transfer function, $A_0(z, f)$ is the frequency and depth-dependent attenuation function in PBS, $H_{\text{s}}^2(z, f)$ is the surface-integrated diffraction function in pulse echo mode and $R(f)$ is the frequency-dependent reflection coefficient of the cartilage surface. Similarly, for the reference interface, the signal S_{ref} can be expressed as

$$S_{\text{ref}}(z, f) = E(f) \times G(f) \times A_0(z, f) \times H_{\text{s}}^2(z, f) \times R_{\text{ref}}(f)\,. \tag{5.2}$$

Equations (5.1) and (5.2) assume that the surface of the sample is uniform, and perpendicular to the direction of the incident ultrasound signal. Furthermore, z has to be large enough 1) compared with the size of the transducer element size to distinguish the attenuation and diffraction and 2) compared with dimensions of the surface insonified by the ultrasound beam.

When the surface diffraction function and the acquisition system characteristics are assumed to be invariable, combining equations (5.1) and (5.2), and assuming that $R_{\text{ref}} \approx 1$, the frequency-dependent reflection coefficient for the cartilage surface reduces to

$$R(f) = \frac{S(z,f)}{S_{\text{ref}}(z,f)}\,. \tag{5.3}$$

The frequency-dependent reflection coefficient is conveniently expressed in decibels as

$$R^{\text{dB}}(f) = 10 \times \log_{10}\langle |R(f)|^2 \rangle\,. \tag{5.4}$$

In this thesis, the spectra $S(z,f)$ and $S_{\text{ref}}(z,f)$ were determined experimentally by delimiting the reflection from the surface of the cartilage in the time domain with a rectangular time window (for the reference signal) or a Hamming window (for the cartilage signal). These time domain signals of equal length were then transformed to the frequency domain by fast Fourier transform (FFT). Finally, the *IRC* was calculated as an integral over the -6 dB frequency bandwidth Δf of the reference spectrum $S_{\text{ref}}(z,f)$ at the focus:

$$IRC = \frac{1}{\Delta f}\int_{\Delta f} R^{\text{dB}}(f)df\,. \tag{5.5}$$

The -6 dB frequency bandwidths Δf were 8 - 20 MHz (in study I) for the 20 MHz transducer, 9 - 47 MHz (in study II) and 8 - 41.5 MHz (in study III) for the 50 MHz transducer, 9 - 14.5 MHz (in study III) and 5.3 to 15.5 MHz (in study IV) for the 10 MHz transducer and 2.7 - 6.3 MHz (in study III) for the 5 MHz transducer.

The definition of the reflection coefficient, *R*, in the time domain includes similar assumptions as used in the definition of the *IRC* (see equations (5.1), (5.2) and (5.3)) and is defined as

$$R = \frac{A_i}{A_i^{\text{ref}}} \times 100\%\,, \tag{5.6}$$

where A_i is the peak-to-peak amplitude of the time-domain ultrasound signal reflected from the cartilage or phantom surface and A_i^{ref} is the peak-to-peak amplitude of the ultrasound signal reflected from the reference interface.

5.4.2 Roughness parameter *URI*

The ultrasound roughness index (*URI* (μm)), analogous to the RMS roughness in material sciences, is determined from the ultrasonically obtained surface profile of a sample [131].

$$URI = \sqrt{\frac{1}{m}\sum_{i=1}^{m}\left(d_i - \langle d\rangle\right)^2}\,, \tag{5.7}$$

where m is the number of the measurement points, *i.e.* A-mode ultrasound signals, d_i is the distance from the transducer to the sample surface at the i:th A-mode signal

and $\langle d \rangle$ is the average distance. The distances d_i were determined from the ultrasound time of flight (TOF) information:

$$d_i = \frac{c \times \text{TOF}}{2}\,, \tag{5.8}$$

where the speed of ultrasound c for the PBS was 1495 m/s [131]. The TOF values were evaluated using the cross-correlation method [21]. The cross-correlation vector was determined using interpolated (cubic interpolation, ratio = 10) ultrasound signals measured from the cartilage surface and from the perfect reflector at a fixed distance. Finally, before calculating the *URI*, the natural surface contour of the cartilage was removed by fitting a smoothing spline to the measured profile and subtracting the contour from the original profile [133]. The smoothing parameter of the spline was manually selected so that the spline function closely followed the general trend of the surface.

5.4.3 Wavelet parameters *MM* and *ED*

Continuous wavelet transform (WT) of a signal x as a function of time t can be expressed as

$$T(a,b) = \frac{1}{\sqrt{a}} \int_{-\infty}^{\infty} x(t)\psi^*\Big(\frac{t-b}{a}\Big)dt\,, \tag{5.9}$$

where a is the dilation parameter or scale, b is the location parameter, ψ is the mother wavelet function and $*$ denotes the complex conjugate [1, 27]. The wavelet transform analysis preserves both the time and frequency information of the original signal. Thus, the wavelet analysis might provide additional information of the cartilage tissue in contrast to only time or frequency domain analysis. In study I, three mother wavelet functions resembling ultrasound reflections from cartilage were chosen for analysis: Morlet, Gaussian and Daubechies (*morl*, *gaus5* and *db6* in the MATLAB wavelet toolbox library, see figure 5.4). In study IV, only *gaus5* was used.

The wavelet coefficients $T(a,b)$ can be plotted to form a wavelet map. For a more explicit presentation, the location parameter b can be converted to time and the scale a can be converted to (pseudo)frequency f:

$$f = \frac{f_c}{a}\,, \tag{5.10}$$

where f_c is the central frequency of the mother wavelet function (see figure 5.5).

The maximum magnitude, *MM* (%) [52], is the largest value in a wavelet transform map, normalized with the largest value in the WT map of the reference signal. The coordinates of the *MM* value in the WT map represent a single (pseudo)frequency component and a single point in time. To calculate the *ED* (μs) [52], the frequency component was fixed, and thus a 2D cross-section of the 3D map at that particular frequency was selected. The Hilbert envelope was then calculated for this 2D signal, and the *ED* was determined as the full width at one tenth of the maximum (FWTM) (in study I) or at the full width at half of the maximum (FWHM) (in study III) of the envelope.

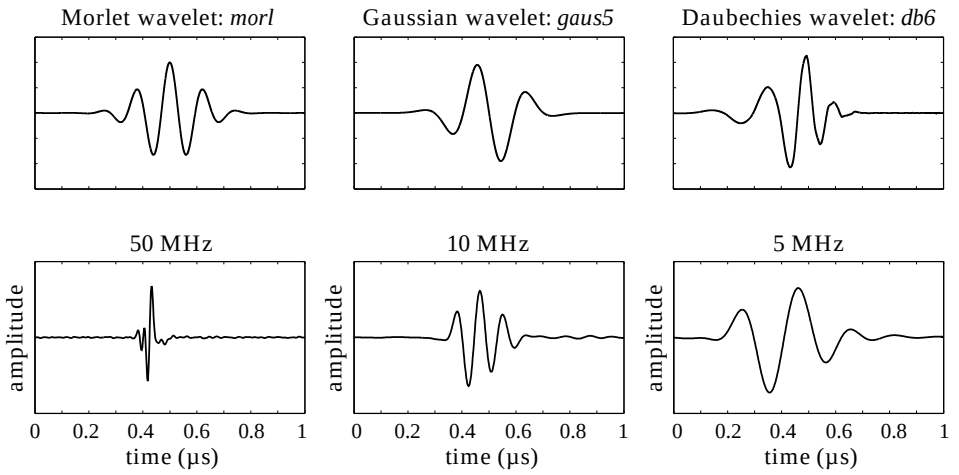

Figure 5.4: The mother wavelet functions selected for study I (top row) and representative ultrasound signals reflected from an intact bovine cartilage surface (bottom row) recorded with the ultrasound transducers used in studies II-IV (see table 5.2).

5.5 Reference methods

Several reference methods were used to relate the values of the calculated ultrasound parameters to the degenerative state of the cartilage tissue or the roughness of the surfaces of the phantoms. The reference methods included light microscopy, scanning electron microscopy, microCT imaging and histological scoring, which are briefly described next.

5.5.1 Light microscopy

Before the ultrasound measuremets in studies II and III, the cartilage surfaces were imaged with a light microscope (Zeiss SV 8, Carl Zeiss Vision International GmbH, Aalen, Germany) to qualitatively estimate the conditions of the surfaces.

After the measurements in all the studies I-IV, microscopic sections (thickness 3 μm) were prepared from the sample as close as practically possible to the region that was measured with ultrasound. The sections were stained with Safranin O for histologic analysis of the samples [74] and imaged with an optical microscope equipped with a CCD camera (Nikon Microphot FXA and Nikon CoolSNAP, Nikon Corporation, Tokyo, Japan). In studies II-IV, all the sections were inspected and one representative histological image per sample was digitized (see figure 5.6). The surface profile was traced on the image manually (in studies II and III) or automatically based on the abrupt changes in the contrast between the cartilage and the background (study IV). The pixel sizes in light microscopy were 4.52 μm (studies II and III) and 3.57 μm (study IV). The RMS roughness values were then calculated from the digitized profiles as a reference for the ultrasonically determined roughness.

Mankin *et al.* have introduced a grading system for histological osteochondral

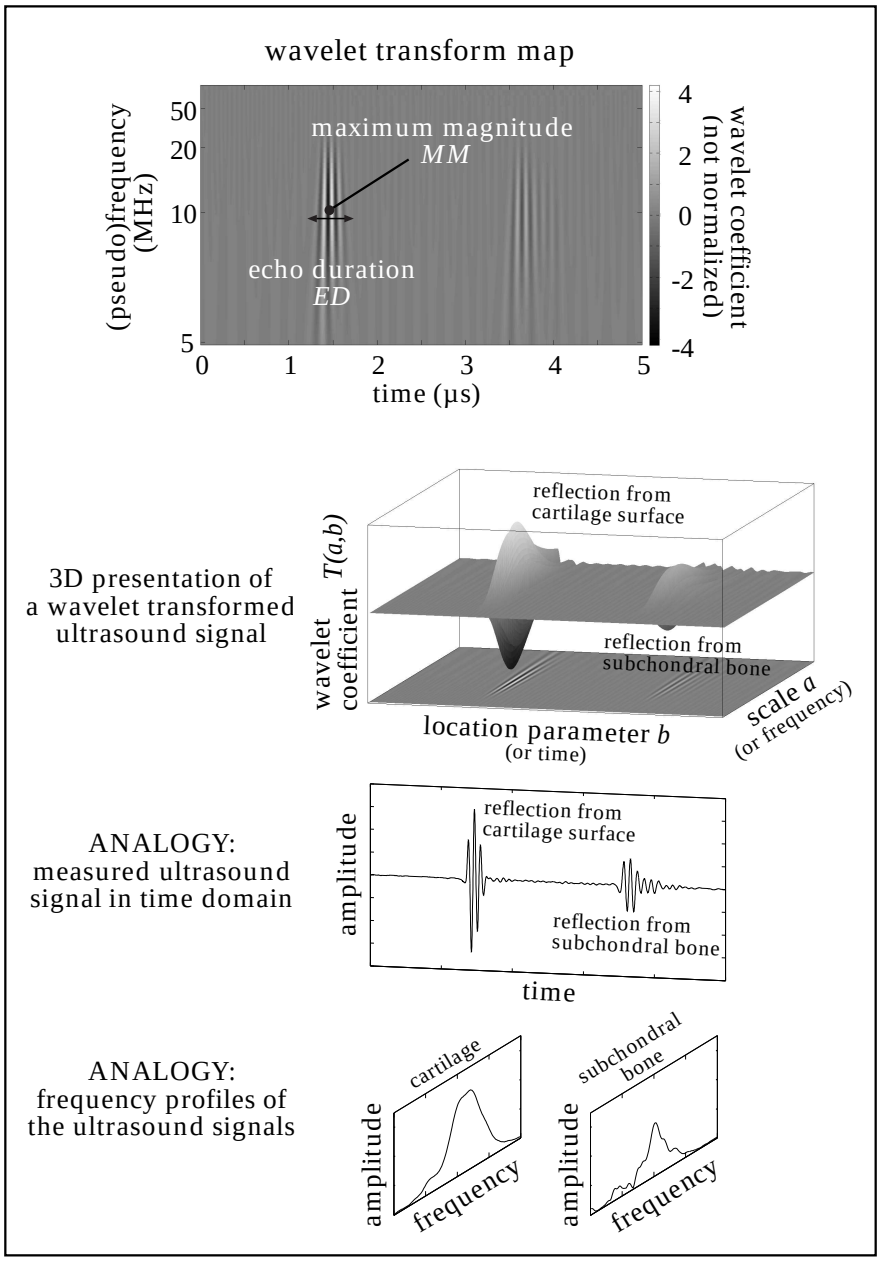

Figure 5.5: Principle of the wavelet transform and determination of the ultrasonic wavelet parameters of articular cartilage.

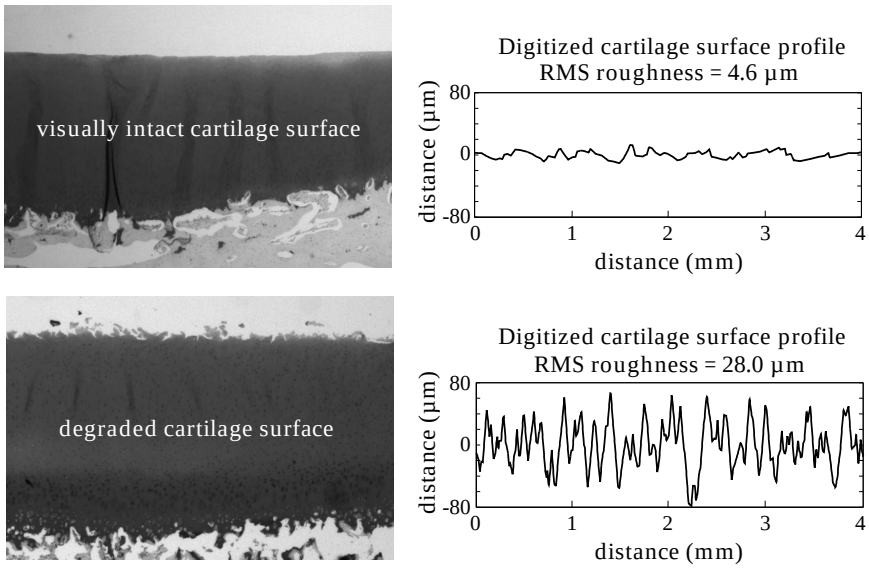

Figure 5.6: Histological sections (left) of intact (top) and degraded (bottom) osteochondral samples and their digitized surface profiles (right).

sections [95]. Table 5.3 lists the factors included in the Mankin score. In this thesis, the Mankin score was used in studies I-III. A Mankin score was assigned for the mechanically degraded cartilage samples also, although the degeneration was artificial. Since the mechanically degraded samples were originally visually inspected as being intact, other signs of degeneration than surface irregularities, such as changes in the cell content and organization, were generally missing.

In study I, the samples were divided into two groups according to their Mankin score: intact (Mankin score = 0) and degenerated (Mankin score = 1-10). In studies II and III, the bovine samples were divided into visually intact and mechanically degraded groups. The Mankin scores in those groups were 0-1 and 1, respectively in both studies. The human samples were awarded Mankin scores 3 and 6 (study II) and 1 and 3 (study III), which correspond to moderate osteoarthritic changes.

In study I, in addition to the Mankin score, the cartilage quality index (CQI) was used. This combines the Mankin score with the water content and dynamic and Young's moduli to reflect the structure, composition, and functional characteristics of the cartilage tissue [109, 113]. The range of the CQI is from 0 for perfectly intact cartilage to 40 for severely degenerated cartilage [109, 113]. The values of the CQI used in study I were extracted from Nieminen *et al.* [109].

5.5.2 Scanning electron microscopy

After the measurements, a half of every sample in studies II and III was prepared for scanning electron microscopy (SEM) (Philips XL30 ESEM, Fei Company, Eindhoven,

Table 5.3: Histological-histochemical grading using Mankin scoring [95]

	Grade		Grade
1. Structure		3. Safranin O staining	
a) normal	0	a) normal	0
b) surface irregularities	1	b) slight reduction	1
c) pannus and surface irregularities	2	c) moderate reduction	2
d) clefts to transitional zone	3	d) severe reduction	3
e) clefts to radial zone	4	e) no dye noted	4
f) clefts to calcified zone	5		
g) complete disorganization	6		
2. Cells			
a) normal	0		
b) diffuse hypercellularity	1	4. Tidemark integrity	
c) cloning	2	a) intact	0
d) hypocellularity	3	b) crossed by blood vessels	1

The Netherlands). Before the SEM imaging, the samples were fixed in 2% glutaraldehyde buffered with 0.1 mol/l cacodylate (pH 7.4), dehydrated in an ascending series of ethanol solutions, dried using the critical point technique, and coated with a sputtered gold layer [69]. The SEM images were used to qualitatively assess the surfaces of the cartilage samples (see figure 5.7).

5.5.3 High-resolution computed tomography

The custom-made phantoms in studies II and III were imaged with a microCT device (computer tomography) (Sky-Scan-1172, SkyScan, Kontich, Belgium)(voltage = 100 kV, filter = 0.5 mm Al) from the region as close as possible to site of the ultrasonic measurements. From the reconstructed slices, the surface profiles were traced and digitized manually and the RMS-roughnesses were evaluated similarly as conducted for the histological cartilage samples. The microCT images were averages of five image frames taken from the same location. The voxel size was $(2.08\ \mu\text{m})^3 \approx 9\ \mu\text{m}^3$.

5.6 Acoustic modeling

In study IV, a sample-specific finite difference time domain (FDTD) model for ultrasonic measurements of articular cartilage in a pulse-echo geometry was developed. The FDTD model for ultrasound reflection from the cartilage surface was constructed using Wave 2000 Plus 3.00 R3 software (CyberLogic Inc., New York, NY, USA). The Wave software solves an acoustic wave equation within each homogenous grid element and computes the displacement vector at each time step of the simulation:

$$\rho\frac{\partial \boldsymbol{w}}{\partial t} = \left[\mu + \eta\frac{\partial}{\partial t}\right]\nabla \boldsymbol{w} + \left[\lambda + \mu + \phi\frac{\partial}{\partial t} + \frac{\eta}{3}\frac{\partial}{\partial t}\right]\nabla(\nabla \cdot \boldsymbol{w})\,, \tag{5.11}$$

where $\boldsymbol{w}$ is a two-dimensional displacement vector, t [s] is time, ρ [kg/m^3] is density, λ [N/m^2] is the first Lamé constant, μ [N/m^2] is the second Lamé constant, η [Ns/m^2]

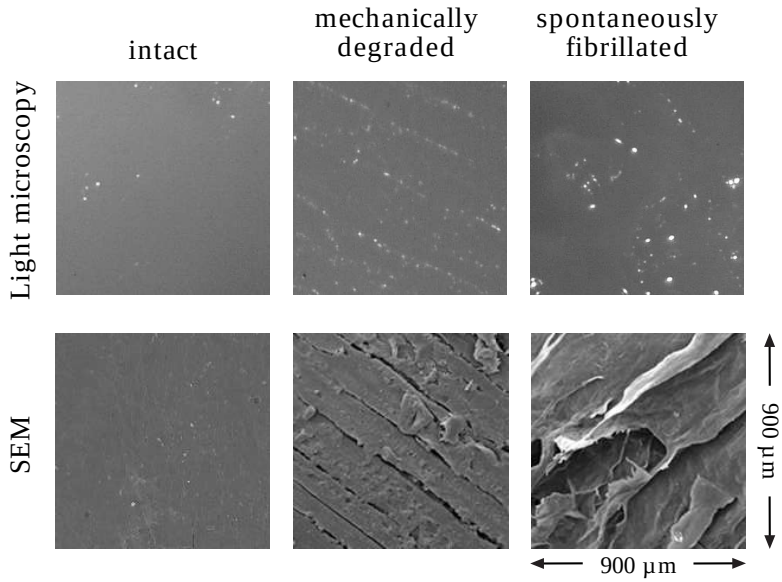

Figure 5.7: Representative images of the articular surfaces of *intact* and *degraded* bovine samples and *spontaneously fibrillated* human sample.

is shear viscosity and ϕ [Ns/m^2] is bulk viscosity. In this equation, isotropy and linear elasticity of the material are assumed.

The model geometry was constructed to be identical with the experimental geometry in study IV (see figure 5.3). This comprised of a non-focused 10 MHz ultrasound transducer and single-phasic homogenous cartilage material immersed in PBS (see figure 5.8). The roughness profiles of the samples, obtained from the digitized histological sections, were implemented in the model individually for each sample. The waveform of the ultrasound signal was digitized from the datasheet of the XMS-310 10 MHz - transducer used in the experimental measurements (see table 5.2). The simulation job parameters were set as follows: time step scale = 1 and point/cycle = 1. The resolving wavelength was set according to the pixel resolution of the model: (280 pix/mm)$^{-1}$ $\approx$ 3.57 μm. This resolving wavelength enabled modeling of ultrasound frequencies up to 15.5 MHz.

The digitized histological human cartilage sections (n = 43) were implemented into the model to simulate the reflection of the ultrasound from cartilage surfaces with a visually intact appearance and with different grades of osteoarthritic surface degeneration. The surface profiles were adjusted to be horizontal by aligning a linear fit of the profile with the horizontal axis. The RMS roughness values of the cartilage surfaces were determined after filtering out the natural curvatures with a smoothing spline fit [133]. The roughness values were in the range of 2 to 64 μm. Young's modulus E was assigned individually to each cartilage sample based on the experimentally obtained values from an earlier study [75]. The density ρ of the cartilage and the longitudinal

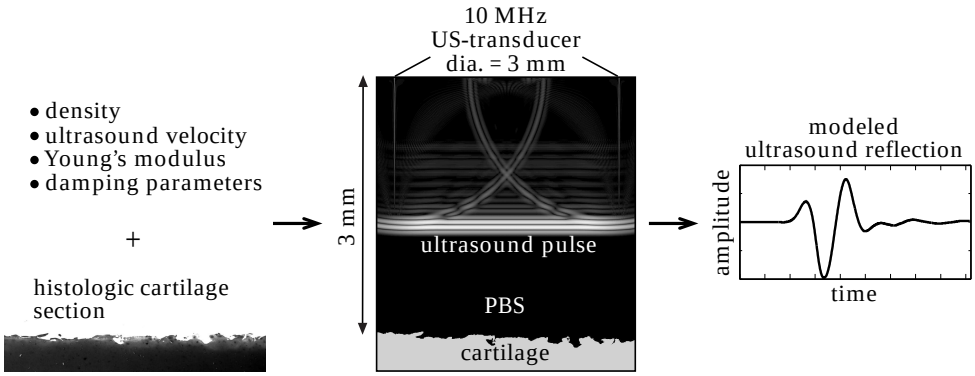

Figure 5.8: Schematic presentation of the model geometry. The cartilage section (middle) has been obtained by thresholding the contrast information of the original histological image (on left).

velocity v_l were fixed at 1000 kg/m^3 and 1600 m/s, respectively. Finally the experimentally determined IRC_{exp} was calculated.

To evaluate systematically the effect of the roughness of the cartilage surface on the integrated reflection coefficient *IRC* (see equation (5.5)), seven artificial roughness profiles were generated (with MATLAB v.7.6.0, The Mathworks Inc. Natick, MA, USA) using a randomized algorithm producing a RMS roughness in a predetermined range around each of the seven desired roughnesses (0.0, 5.1, 7.8, 13.1, 26.2, 28.8 and 29.7 μm). The roughness values selected for the artificially created cartilage surface profiles corresponded to the roughness values reported for early degeneration of cartilage [2, 24, 39, 104, 133]. The IRC_{model} was calculated from the modeled data obtained for the seven roughnesses with eleven different combinations of the values for material parameters: longitudinal velocity (v_l), density (ρ) and Young's modulus (E) (table 5.4).

The values of the material parameters were chosen so that they correspond to the realistic range of the parameter values for articular cartilage. The selected range of the v_l was from 1500 m/s to 1700 m/s [3, 111, 143]. The ρ was estimated to range between 1000 kg/m^3 and 1100 kg/m^3 [67]. Dynamic moduli in a range from about 2 MPa [84] to about 240 MPa have been reported [19]. Based on this, Young's modulus E was set to vary between 0 MPa and 100 MPa in the simulations.

Three combinations of the values of the material parameters v_l, ρ and E were selected (materials 1, 5 and 10 in table 5.4) to study the effect of inclining the surface of the cartilage with respect to the direction of the ultrasound beam. The aforementioned seven artificial roughness profiles were inclined by steps of 1° from -5° to 5°, the 0° corresponding to the position where the direction of the ultrasound beam was normal to the surface profile. Again, the IRC_{model} was determined.

Table 5.4: Combinations of the values of the material parameters for the artificial cartilage samples used in the acoustic model. Young's modulus E, longitudinal velocity v_l and density ρ were used to calculate the Lamé constants λ and μ. The viscous damping parameters η (shear viscosity) and ϕ (bulk viscosity) were set to constant values of 1.75 Ns/m^2 and 199.7 $\times$ 10^{-6} Ns/m^2, respectively.

material	E (MPa)	v_l (m/s)	ρ (kg/m^3)	λ (MPa)	μ (MPa)
0	0	1500	1000	2250.0	0.0
1	10	1525	1010	2342.7	3.3
2	20	1550	1020	2438.2	6.7
3	30	1575	1030	2536.5	10.0
4	40	1600	1040	2637.7	13.4
5	50	1625	1050	2741.8	16.7
6	60	1650	1060	2848.8	20.0
7	70	1675	1070	2958.7	23.4
8	80	1700	1080	3071.7	26.7
9	90	1725	1090	3187.7	30.1
10	100	1750	1100	3306.9	33.4

5.7 Statistical analyses

All statistical analyses in studies I-IV were conducted using SPSS 14.0 program (SPSS INC., Chicago, IL, USA).

In study I, the relationships between the continuous ultrasound parameters and the discrete cartilage scoring parameters (the CQI and Mankin score) were investigated using the Spearman's correlation analysis. The Mann-Whitney U test was used to detect statistically significant differences in the ultrasound parameter values between the *intact* and *degenerated* cartilage groups. The reproducibilities of the *ED* and *MM* were determined by analyzing three repeated measurements of eight intact samples and quantified by determining coefficients of variation (CV). Receiver operating characteristic (ROC) analysis was used to determine the cutoff value, sensitivity and specificity of the ultrasound parameters. Stepwise linear regression analysis was used to determine which ultrasound parameters predicted the value of the Mankin score.

In study II, Wilcoxon signed rank test was done within the cartilage groups *intact* and *mechanically degraded* to see whether there were statistically significant differences between the parameter values obtained in different angles of incidence (0°, 2°, 5° and 7°). Mann-Whitney U test was conducted to detect statistically significant differences between the parameter values obtained in the normal incidence (0°) of the *mechanically degraded* group and in 0°, 2°, 5° or 7° angle of incidence of the *intact* group.

In study III, the Mann-Whitney U test was used to detect statistically significant differences in the ultrasound parameter values between the *intact* and *mechanically degraded* cartilage groups. The Wilcoxon signed ranks test was used to evaluate the effects of altering the ultrasound frequency, temporal sampling frequency and spatial sampling step.

In study IV, Spearman's correlation coefficients were determined for the comparisons between ultrasound parameters and reference roughness values. The mixed

linear model was used to investigate the statistical significance of spatial variation of the IRC_{exp} values between the different measurement sites on the healthy and degenerated patellae.

CHAPTER VI

Results

The most important results of the studies I - IV are summarized in this chapter. The complete results are presented in the original studies I - IV.

6.1 Comparison of ultrasound parameters in time, frequency and wavelet domains

All ultrasound parameters evaluated in study I (*IRC*, *R*, *URI*, *MM* and *ED*) were able to differentiate the *intact* samples from the *degenerated* bovine cartilage samples (table 6.1). The choice of the mother wavelet (*morl*, *db6* or *gaus5*) (see figure 5.4) had a minor effect on the absolute values of the *ED*, but almost no effect on the *MM*. The sensitivity of the *ED* in detecting cartilage degeneration depended on the chosen mother wavelet also, whereas the sensitivity of the *MM* remained almost constant. The reproducibility was good for both the *MM* (CV = 4.9% - 5.1%) and the *ED* (CV = 0.3% - 1.3%) and it was only slightly dependent on the choice of the mother wavelet.

Significant correlations (r = 0.669 - 0.833, (r^2 = 0.448 - 0.694,) $p < 0.01$) were established between all the ultrasound parameters and the cartilage scoring parameters, *i.e.* the CQI and the Mankin score (table 6.1). The wavelet parameters *MM* and *ED* did not improve the ability to predict the value of the Mankin score compared with the linear combination of only the *URI*, *R* and *IRC* (stepwise linear regression, r = 0.842 , $p < 0.0001$). The specificities of all the parameters were excellent and the sensitivities to the degeneration of the cartilage were also good (table 6.1).

6.2 Effects of articular surface roughness on ultrasound parameters

In all experimental ultrasound measurements of studies I - IV, the roughness of the cartilage surface (spontaneous or mechanically induced roughening) affected all the ultrasound parameters. The effect of the surface roughness on the ultrasound parameters was evaluated systematically with phantoms (in study III) and by numerical modeling (in study IV).

The *URI* distinguished between the *intact* and *degraded* bovine cartilage groups in studies I,II and III. Furthermore, in studies II and III, with the 50 MHz ultrasound transducer, the *URI* was effective in reproducing the "true" roughness values evaluated from the safranin O stained microscopic slices (for cartilage) or microCT profiles

Table 6.1: Mean values of the ultrasound parameters ($\pm$ SD) and their specificities, sensitivities and Spearman's correlations with the cartilage scoring parameters for *intact* and *degenerated* cartilage groups. All ultrasound parameters differentiated between the cartilage groups.

	average (n = 11): intact	average (n = 21): degenerated	specificity	sensitivity	correlation with Mankin score	correlation with CQI
R (%)	5.3 $\pm$ 0.9	2.4 $\pm$ 1.7*	1.00	0.86	-0.833	-0.745
IRC (dB)	-26.7 $\pm$ 1.6	-34.1 $\pm$ 5.5*	0.91	0.86	-0.826	-0.752
URI (μm)	7.4 $\pm$ 1.2	24.2 $\pm$ 15.5*	1.00	0.91	0.825	0.693
MM_{gaus5} (%)	4.6 $\pm$ 0.9	2.2 $\pm$ 1.5*	1.00	0.76	-0.799	-0.747
ED_{gaus5} (μm)	0.18 $\pm$ 0.01	0.29 $\pm$ 0.10*	1.00	0.86	0.823	0.669

* Statistically significant difference ($p < 0.001$, Mann-Whitney U test) in the ultrasound parameter values was detected between the *intact* and *degenerated* cartilage sample groups for all the ultrasound parameters.

(for phantoms). However, in study III, it was observed that the *URI* revealed the differences in the roughnesses of the surfaces of the phantoms and between the *intact* and *degraded* cartilage groups only when determined with the focused 50 MHz transducer.

In studies I - IV, the reflection parameters R and IRC detected spontaneous or mechanically induced roughening of the cartilage surface. In study IV, the dependence of the IRC_{model} on the artificially generated surface roughness was very similar with different combinations of the values of the material parameters (table 6.2). When the roughness of the surface of the cartilage was increased from 0 μm to $\sim$30 μm, the change in the values of the IRC_{model} was from -8 to -14 dB for any chosen combination of the values of the material parameters. To obtain the same change in the values of the IRC_{model} by changing the values of the material parameters, Young's modulus E would have to change by about 80 MPa, the longitudinal velocity v_l by about 200 m/s and the density ρ by about 80 kg/m^3.

Table 6.2: The values of IRC_{model} (dB) as a function of the surface roughness for different combinations of the values of the material parameters (see table 5.4). The values of the IRC_{model} decrease as the roughness of the surface increases for all combinations of the values of the material parameters.

material (see table 5.4)	roughness (μm) 0.0	5.1	7.8	13.1	26.2	28.8	29.7
1	-24.0	-27.5	-27.0	-36.6	-37.5	-36.4	-35.4
5	-13.4	-16.8	-16.9	-31.1	-31.2	-28.9	-26.9
10	-8.0	-11.3	-11.6	-26.4	-26.9	-22.8	-20.8

In study IV, the correlation between the IRC and the "true" roughness of the human samples was significant (r = -0.574, $p < 0.01$ for IRC_{exp} and r = -0.523, $p < 0.01$ for IRC_{model}) (figure 6.1). However, the correlation between the experimentally and numerically determined values of the IRC was very weak (r = 0.155, p = 0.320) (figure 6.1).

In the experimental cartilage data from study III, no correlation was found between the "true" roughness of the cartilage surface, evaluated from the safranin O

stained microscopic slices, and the *IRC* (figure 6.2). There was no correlation between the "true" roughness and the *URI* either (figure 6.2). However, a good correlation was obtained between the ultrasonically determined roughness, *URI*, and the *IRC* (figure 6.2). For the phantoms the "true" roughness was evaluated from the microCT profiles and the Spearman's correlation coefficients were -0.900 (roughness vs. *IRC*), 1.000 (roughness vs. *URI*) and -0.900 (*URI* vs. *IRC*).

The *MM*, which closely corresponds to the *R* (r = 0.815 - 0.982, $p < 0.01$), detected variation in the roughnesses of the phantoms and the degradation of the superficial cartilage ($p < 0.01$, Mann-Whitney U test) in study III. The *ED* was rather insensitive to the changes in the surface characteristics of the samples.

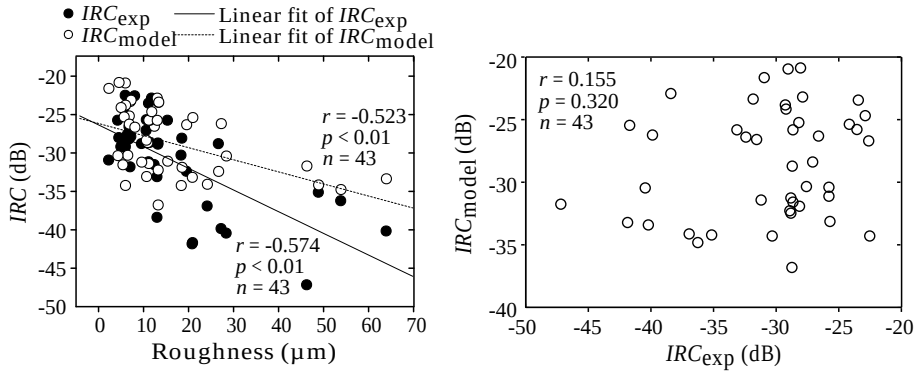

Figure 6.1: Linear correlations between the surface roughness of the human samples and the experimentally and numerically evaluated (with 10 MHz unfocused ultrasound transducer) integrated reflection coefficients IRC_{exp} and IRC_{model} (data from study IV).

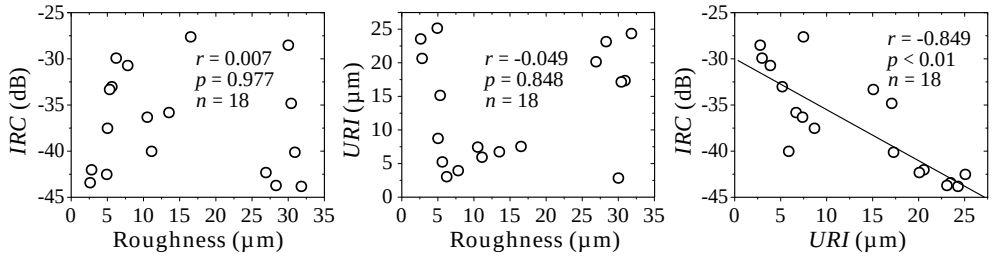

Figure 6.2: Linear correlations between surface roughness, *URI* and *IRC* evaluated with 50 MHz focused ultrasound transducer for bovine cartilage (unpublished data from study III).

6.3 Effects of ultrasound angle of incidence on ultrasound parameters

The effects of angle of incidence of the ultrasound beam with respect to the surface of the sample on the ultrasound parameters was investigated experimentally with cartilage samples (in study II) and by modelling the ultrasound reflection from cartilage tissue with artificial surface profiles (in study IV).

In study II, the angle of incidence of the ultrasound beam affected the values of the ultrasound parameters less in the *degraded* group than in the *intact* group ($p < 0.05$). When the surface of the sample was inclined from 0° to 7°, the values of the *IRC* decreased from -29.0 dB to -42.9 dB in the *intact* cartilage group and from -45.5 dB to -48.9 dB in the *degraded* cartilage group (figure 6.3). Inclining the surface also affected the *URI*, which increased from 6.4 μm to 19.3 μm in the *intact* group and from 21.7 μm to 32.7 μm in the *degraded* group (figure 6.3). The changes in the *IRC* and the *URI* were statistically significant ($p < 0.05$). The angular dependence of the *URI* was rather similar in both the *intact* and *degraded* groups.

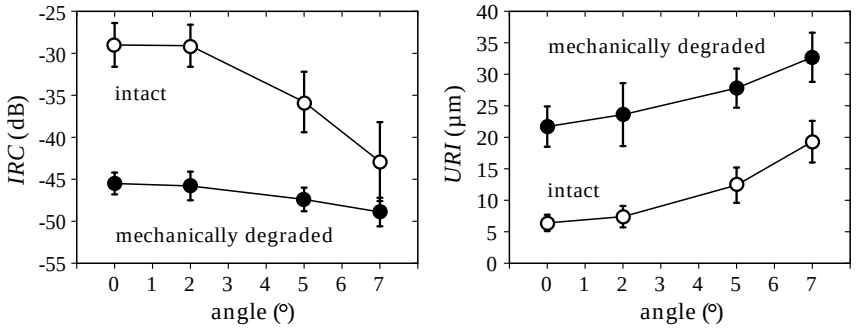

Figure 6.3: Angular dependence of the *IRC* and the *URI* determined with the 50 MHz ultrasound transducer (data from study II).

In study II, the values of all ultrasound parameters of a spontaneously fibrillated human cartilage sample (Mankin score = 6, *i.e.* moderate degeneration) in any angle of incidence differed from the values of the intact samples examined at a normal angle of incidence, and thus the fibrillated sample could always be distinguished. The *URI* could even discern the fibrillated sample irrespective of the angles of incidence of the fibrillated *and* the intact samples. Furthermore, all the ultrasound parameters distinguished ($p < 0.05$) the *mechanically degraded* group from the *intact* group regardless of the change in the angle of incidence of the degraded samples, up to an angle of incidence of 5° of the intact samples.

In the *intact* group, the values of the *R* and the *IRC* in 0° angle (normal incidence) were distinguished ($p < 0.05$) from the values in the 5° and 7° angles of incidence. In the *degraded* group, only the values of the *R* and the *IRC* in the 7° angle of incidence were distinguishable ($p < 0.05$) from the values of the *R* and the *IRC* in the normal incidence (0°). Furthermore, in the *intact* group, the values of the *URI* in the normal

incidence (0°) could be distinguished from values of the *URI* in all the other angles of incidence (2°, 5° and 7°). In the *degraded* group, the values of the *URI* in the 5° and 7° angles of incidence were differentiatable from the values of the *URI* in the 0° angle.

In study IV, a strong angular dependence of the IRC_{model} was found for the perfectly smooth cartilage surface for all three chosen combinations of the values of the material parameters (figure 6.4). A threshold between the roughness values 7.8 μm and 13.1 μm was found, beyond which, when the roughness increased, the reflection of the ultrasound strongly diminished and the angular dependence of the reflection seemed to disappear (figure 6.4).

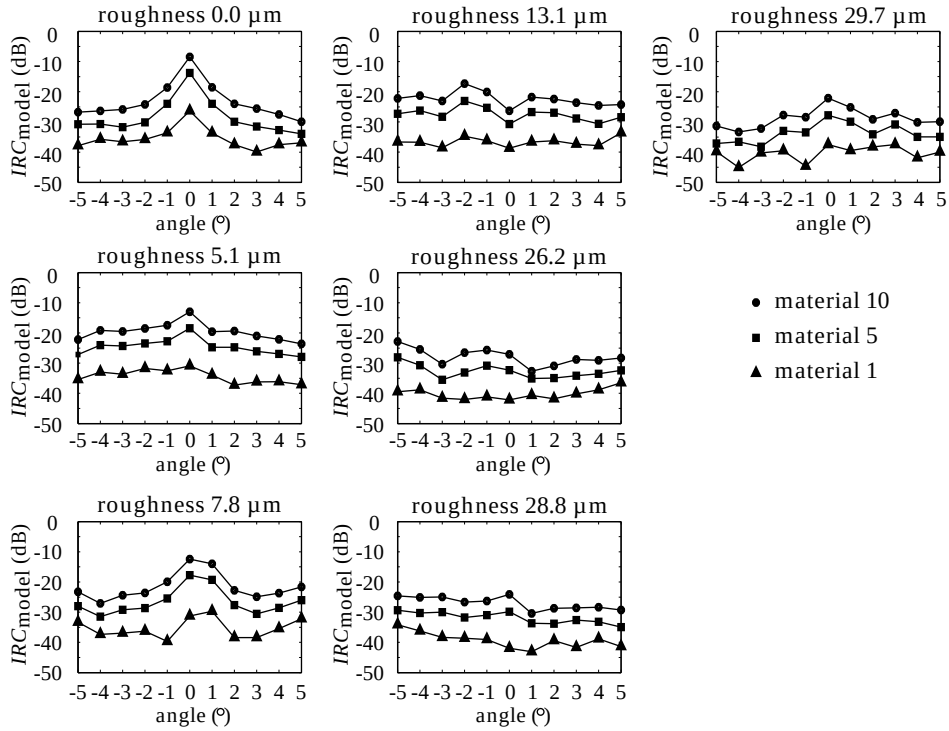

Figure 6.4: The angular dependence of IRC_{model} for three combinations of the values of the material parameters (see table 5.4) and different values of surface roughness determined with the 10 MHz ultrasound FDTD model.

6.4 Effects of ultrasound frequency, temporal sampling frequency and spatial sampling step on ultrasound parameters

In study III, the effects of ultrasound frequency and focusing, temporal sampling frequency and spatial sampling step were investigated. The results for the *URI*, the *IRC* and the *ED* evaluated with three different ultrasound transducers are summarized in table 6.3. The values of the *R* and the *MM* are omitted from table 6.3, because the results for the *R* and the *MM* were in close agreement with those of the *IRC*.

Table 6.3: Values of ultrasound parameters, determined using frequencies 50, 10 and 5 MHz, for phantoms and cartilage samples with different surface characteristics. The differences in the roughnesses of the phantoms are revealed only with the 50 MHz transducer.

Ultrasound frequency	polished steel	smooth phantom	P360	P240	P120	P60	intact (n = 8)	degraded (n = 8)
50 MHz								
URI (μm)	0.2	1.3	6.3	9.6	27.7	33.2	5.3 ± 2.1	$20.9 \pm 3.5^{***}$
IRC (dB)	-1.3	-14.1	-27.6	-33.7	-37.6	-36.2	-34.2 ± 4.1	$-41.6 \pm 3.5^{**}$
ED (μs)	0.07	0.06	0.09	0.11	0.11	0.12	0.08 ± 0.02	$0.14 \pm 0.02^{***}$
10 MHz								
URI (μm)	0.7	0.4	0.8	0.9	24.9	23.5	1.1 ± 0.3	1.3 ± 0.3
IRC (dB)	-0.1	-23.2	-24.6	-32.6	-41.5	-52.0	-36.4 ± 6.2	$-45.8 \pm 4.7^{*}$
ED (μs)	0.19	0.20	0.19	0.19	0.41	0.26	0.20 ± 0.03	0.20 ± 0.05
5 MHz								
URI (μm)	0.9	0.3	0.9	0.8	3.2	3.7	1.1 ± 0.3	1.5 ± 0.3
IRC (dB)	-0.1	-20.8	-22.6	-23.4	-33.0	-37.9	-32.5 ± 2.5	$-36.5 \pm 1.4^{**}$
ED (μs)	0.26	0.29	0.28	0.29	0.33	0.34	0.29 ± 0.03	0.32 ± 0.03

* $p < 0.05$, ** $p < 0.01$, *** $p < 0.001$. Statistically significant difference between the parameter values obtained in the *intact* and *degraded* sample groups determined by Mann-Whitney U test.
The mean particle sizes of the emery papers used to cast the phantoms are 40.5 μm (P360), 58.5 μm (P240), 125 μm (P120) and 269 μm (P60).

At the ultrasound frequencies of 5 MHz and 10 MHz, the *URI* failed to differentiate the surface roughnesses of the phantoms from each other and between the cartilage sample groups (table 6.3, figure 6.5). The type of ultrasound transducer in use affected the values of the *URI* significantly ($p < 0.05$, for phantoms, $p < 0.01$ for cartilage), except between the 5 MHz and 10 MHz transducers.

In the cartilage measurements, the *R*, the *IRC* and the *MM* detected mechanically induced degradation of the surface at all the investigated frequencies ($p < 0.05$)(table 6.3). The *ED* was not as sensitive, and with 10 MHz and 5 MHz, the *intact* and *degraded* cartilage groups were not distinguished. The type of the ultrasound transducer affected the values of the *R*, the *IRC* the *MM* and the *ED* significantly ($p < 0.05$, for phantoms, $p < 0.01$ for cartilage).

Altering the size of the spatial sampling step only affected the *URI* ($p < 0.05$ for phantoms, $p < 0.01$ for cartilage). However, although the absolute values of the *URI* increased as the size of the spatial sampling step increased, the differences between the phantoms and between the cartilage groups were discernible ($p < 0.05$) with all sampling steps (table 6.4). Decreasing the temporal sampling frequency affected the values of all the investigated ultrasound parameters of the cartilage samples ($p < 0.01$) and the values of the *R* and *ED* of the phantoms ($p < 0.05$) significantly. However, the *intact* and *degraded* cartilage groups could always be distinguished.

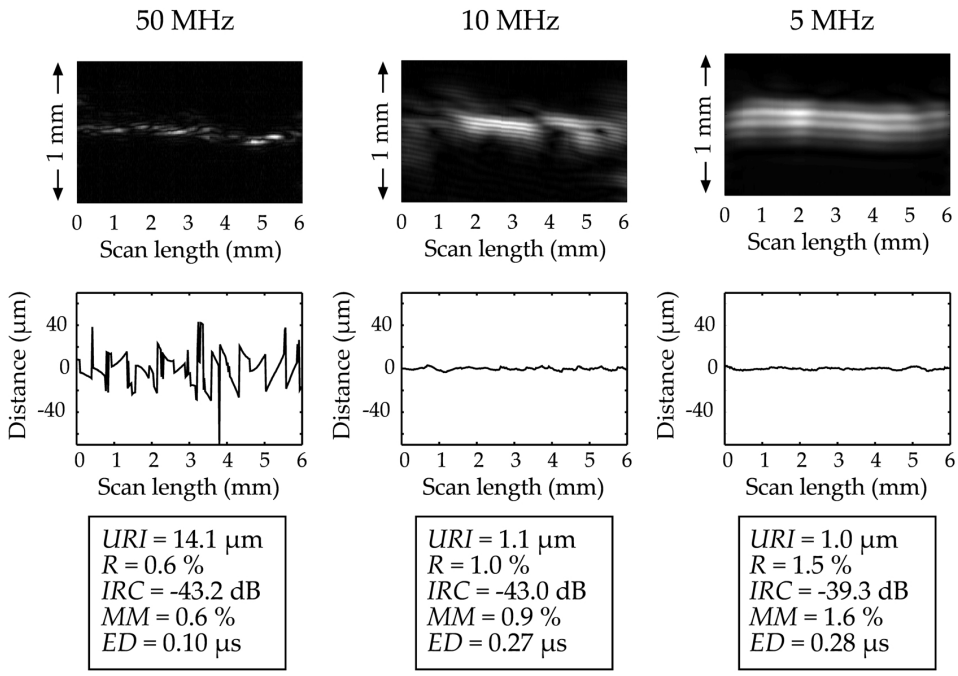

Figure 6.5: B-mode ultrasound images (top) and corresponding ultrasonically determined surface profiles (middle) of one degenerated cartilage sample evaluated using 50 MHz, 10 MHz and 5 MHz ultrasound transducers. Values of ultrasound parameters determined at each frequency are listed (bottom).

Table 6.4: The *URI* for phantoms and cartilage samples with different spatial sampling steps determined with the 50 MHz ultrasound transducer. Increasing the spatial sampling step affected the *URI* significantly, while the other parameters remained unaffected.

Step size (μm)	polished steel	smooth phantom	P360	P240	P120	P60	intact (n = 8)	degraded (n = 8)
20	0.2	1.3	6.3	9.6	27.7	33.2	5.3 ± 2.1	$20.9 \pm 3.5^{***}$
60	0.3	2.0	7.9	11.5	36.2	44.1	7.6 ± 2.4	$25.6 \pm 4.4^{***}$
120	0.3	3.2	9.2	13.0	41.1	46.2	11.2 ± 5.4	$27.7 \pm 4.6^{***}$
240	0.4	3.8	10.2	19.0	38.3	60.5	16.8 ± 10.7	$28.9 \pm 5.2^{*}$

* $p < 0.05$, *** $p < 0.001$. Statistically significant difference between the parameter values obtained in the *intact* and *degraded* sample groups determined by Mann-Whitney U test.
The mean particle sizes of the emery papers used to cast the phantoms are 40.5 μm (P360), 58.5 μm (P240), 125 μm (P120) and 269 μm (P60).

CHAPTER VII

Discussion

In this thesis, quantitative ultrasound imaging (QUI) parameters of articular cartilage were assessed in terms of their ability to detect the characteristic signs of cartilage degeneration in early osteoarthrosis. In study I, parameters based on time domain, frequency domain and wavelet transform (WT) analyses were compared. In study II, the effects of non-perpendicular ultrasound angle of incidence on the QUI parameters were investigated. In study III, the effects of ultrasound frequency, temporal sampling frequency and size of the spatial sampling step on the QUI parameters were studied. In study IV, an FDTD model for the ultrasound reflection from the surface of articular cartilage was constructed to evaluate the effects of varying surface roughness, material parameters and inclination of the cartilage sample on the QUI parameters.

7.1 Time, frequency and wavelet domain parameters

All QUI parameters investigated in study I correlated with the structure, composition and mechanical properties of articular cartilage. The linear correlation of the QUI parameters was better with the Mankin score than with the cartilage quality index (CQI). This is probably explained by the fact that the samples displayed predominantly superficial changes, such as fibrillation, and thus the Mankin scores (see table 5.3) were low (0-10/14, mean 2.8, mode 0). The CQI, on the other hand, takes into account also the water content and the dynamic and Young's moduli of the cartilage, which reflect the properties of the bulk tissue. Thus, the CQI is not as sensitive to the superficial changes as the Mankin score.

The *URI*, by definition, is determined from multiple A-mode ultrasound reflections. The other QUI parameters can, in principle, be evaluated from a point measurement. In practice, however, parameters from multiple adjacent A-mode data acquisitions should be averaged to obtain more representative results.

The WT parameters provided no additional information compared with the *R*, *IRC* and *URI*. Hence, the results suggest that the relatively simple time-domain parameters (the *R* and the *URI*) are diagnostically as sensitive as the more complex frequency-domain (*IRC*) or wavelet trasform (the *MM* and the *ED*) parameters. Indeed, in study III, the strong linear correlation (r = 0.815 - 0.982, $p < 0.01$) between the *R* and the *MM* proved that the information manifested by those parameters is essentially the same and, thus, the calculation of the more complex wavelet parameter might not be relevant.

The complexity of the WT parameters may even hinder real-time clinical analysis. Sophisticated and thus a probably time-consuming algorithm for quantifying the *ED* would be needed in order to minimize the effects of fluctuation and impulse noise of the ultrasound signal if it were to be included in an automated clinical application. The values of the *ED* even for intact cartilage corresponded to > 320 μm depth, assuming a speed of sound of 1600 m/s for the cartilage. Thus, the *ED* does not directly represent the "true" roughness of the surface, whereas the *URI* was found to correspond more closely to the microscopically determined roughness in studies I, II and III. Furthermore, in degenerated cartilage, the values of *ED* showed significant variation between different transducer positions. Therefore, the *ED* value must be interpreted carefully [157]. In study III, the changes in the *ED* between the *intact* and *degraded* sample groups were not distinguishable with the lower frequencies, because the long pulse lengths obscured any changes related to superficial degeneration.

The current WT assessment of articular cartilage can extract the *MM* and *ED* values freely corresponding to different (pseudo)frequencies. Since the acoustic properties of cartilage depend on the structure and composition of the tissue, validation of the *MM* and *ED* at certain fixed frequencies might provide more specific information on the integrity of the articular cartilage and improve the reproducibility of the parameters. If developed further, the WT analysis might provide some additional information compared with separate analyses in the time or frequency domains for the determination of the properties of the cartilage-bone interface, due to its ability to preserve the time and frequency information simultaneously.

7.2 Effects of articular surface roughness on ultrasound results

In study III, the *URI* value determined with the focused 50 MHz ultrasound transducer for the polished steel surface was 100 nm and for intact cartilage it was about 4.8 ± 1.7 μm. A surface roughness of 10 nm has been reported for polished steel measured with a surface profilometer [142], and 0.8 ± 0.2 μm for intact cartilage determined with laser profilometry [39]. The results are consistent, if the measuring limit of the present ultrasound system and limitations of the analysis techniques are taken into account. In all ultrasound systems, there is always some noise that affects the ultrasound signals. Furthermore, since the -6 dB width of the 50 MHz ultrasound beam is 120 μm (table 5.2) and the wavelength of the ultrasound is around 30 μm, it is not possible to detect roughness differences in the nanometer scale using an ultrasound transducer. However, the resolution is sufficient to quantify pathological increase in the roughness of the cartilage surface [104].

Although the values of the *URI* for the cartilage surfaces were within the same range as the "true" roughnesses evaluated from the microscopic slices, there was no correlation between the *URI* and the "true" roughness (r = -0.049)(figure 6.2). The major factor responsible for the lack of correlation was probably the difference in the spatial location of the ultrasound and microscopic measurements. Furthermore, some discrepancy between the *URI* and "true" roughness may arise from the artifacts caused by preparation of the cartilage slices for microscopy. This speculation is supported by the result that the correlations for the phantoms between the *URI* and "true" roughness extracted from microCT images were excellent (r = 1.000). In the microCT imaging, no sample processing is needed and thus the image artifacts are

practically negligible.

In study IV, the "true" surface roughness of the human cartilage samples correlated moderately with the IRC_{exp} determined experimentally (r = -0.574) and with the IRC_{model} extracted from the numerical FDTD model (r = -0.523). However, the poor correlation between the IRC_{exp} and IRC_{model} (r = 0.155) suggests that, in addition to the roughness, the material parameters also contribute significantly to the value of the *IRC* (figure 6.1). It can be seen from figure 6.1, that corresponding to a narrow roughness range (*e.g.* 1 -2 μm), there can be many different values of the experimental IRC_{exp}. This also suggests that the absolute values of the IRC_{exp} are affected by the intrinsic material properties of the cartilage. The water content and, thus, the density of the cartilage probably had a major impact on the *IRC*, because in the model the density was fixed whereas in the experimental measurements its value varied. With the phantoms, the roughness was the major factor causing differences in the *IRC*, because the phantoms were all made of the same homogeneous and isotropic material (hot-setting adhesive).

In study III, there was no correlation between the "true" roughness and the *IRC* of the cartilage samples (r = 0.007, p = 0.977, n = 18) (figure 6.2). The discrepancy compared with the results of study IV might arise from the more sophisticated digitizing of the roughness profiles from the microscopic slices in study IV. However, the same digitizing procedure of the surface profile was used for the phantoms and the correlation between the "true" roughness and the *IRC* for the phantoms was higher (r = -0.900, p = 0.037, n = 5). Thus, the discrepancy in the cartilage measurements is more likely to be due to the spatial difference between the ultrasonic and microscopic measurement sites and processing artifacts in the microscopic cartilage sections rather than by being attributable to the digitizing process.

In study III, it was confirmed that the focusing and the frequency of the ultrasound transducer could affect the ability of the ultrasound method to detect the roughness of the surface of the sample - generally, a focused transducer with a sufficiently high frequency is needed. Therefore, if a focused transducer had been used in the modeling in study IV, the relative effect of the roughness on the ultrasound reflection might have been greater than the effect of the material parameters.

7.3 Significance of ultrasound angle of incidence on ultrasound results

In study II, the angle of incidence of the ultrasound beam affected all investigated ultrasound parameters significantly ($p < 0.05$). For the *intact* samples, the *R* and the *IRC* decreased significantly as a function of the angle of incidence of the ultrasound beam, but the angular dependence was not so pronounced with the degraded or fibrillated samples (figure 6.3). This may be explained by the different contributions of specular reflection and scattering, the latter being more dominant at a fibrillated cartilage surface [23, 141]. This conclusion is also supported by the fact that the ultrasound signal reflected from the polished steel surface decreased rapidly as a function of the angle of incidence.

In study II, the *URI* was less susceptible to the increase in the angle of incidence than the *R* or the *IRC* (figure 6.3). Nonetheless, the angular dependence of the *URI*

was detectable and might have been caused by a deterioration in the signal-to-noise ratio and changes of the pulse shape of the ultrasound signal at the higher angles of incidence. In study IV, when the roughness of the cartilage surface was increased, the angular dependence of the IRC_{model} disappeared between the roughness values of 7.8 μm and 13.1 μm (figure 6.4). This supports the conclusion of study II that scattering may be a more dominant phenomenon than the specular reflection from the surface of the degenerated cartilage.

In study IV, a threshold of about 2° in the angle of incidence was found, beyond which the values of the IRC_{model} became nearly constant, probably because of increased proportion of scattering (compared with specular reflection) and the decrease of the signal-to-noise ratio (figure 6.4). It is, however, significant that in study II, the *degraded* samples were distinguished from the *intact* ones up to an angle of incidence of 5° for the intact samples.

If minor fibrillation of a cartilage surface is to be detected reliably with the present QUI parameters, the angle of incidence of the ultrasound beam has to be carefully controlled in the measurements. In a clinical measurement, the natural curvature of the articular surface varies also, and it may be challenging to achieve perfect perpendicularity between the ultrasound beam and the surface of the cartilage. Consequently, a mathematical correction based on estimating the angle of incidence from the ultrasound echo information might be valuable. However, the proportions of ultrasound reflection and scattering change as a function of the angle of incidence. Furthermore, the proportion of scattering probably increases as a function of the surface fibrillation of the cartilage. Thus, mathematical correction of the angle of incidence might not be straightforward in the case of the reflection parameters *R* and *IRC*.

7.4 Effects of measurement parameters on ultrasound results

The *URI* values determined with the 50 MHz ultrasound transducer were in the same range as the reference roughness values determined from the microCT or histological images of the phantoms (study III) and the cartilage samples (studies II and III), respectively. However, at the lower frequencies (5 and 10 MHz), the *URI* was insensitive to changes in the reference roughness probably due to an increased pulse length and a wider beam diameter. Thus, one advantage of using high ultrasound frequency ($\sim$50 MHz) is the short pulse duration. This reduces the possibility of complications, due to the alteration of the shape of the reflected ultrasound signal, in the determination of the surface profile using the cross correlation method used in the calculation of the *URI*.

The *ED* was also insensitive to the surface characteristics of the cartilage at the low frequencies (5 and 10 MHz) and did not separate the cartilage groups at those ultrasound frequencies. In contrast to the other QUI parameters, the *ED*, by definition, depends on the properties of the ultrasound transducer, especially on the pulse duration. Therefore, a comparison of the values of the *ED* between the ultrasound frequencies and transducers is irrelevant.

The ultrasound reflection parameters *R*, *IRC* and *MM* detected the cartilage degradation also at the low ultrasound frequencies. Ultrasound reflection and backscattering at 5 MHz QUI have been reported to be strongly related to the structure, composition, density and mechanical properties of the bone [47, 57]. This is important

because both the cartilage and subchondral bone are affected in the OA process [18] and application of low ultrasound frequencies (∼5 MHz) could enable simultaneous diagnosis of the properties of both tissues. Monitoring the changes in the subchondral bone would also be useful for evaluating the healing of a cartilage injury *e.g.* after surgical repair [145].

According to earlier studies, enzymatic PG depletion has no significant effect on the ultrasound reflection from the surface of the cartilage [83, 111, 123, 144]. This is supported by our finding in study III that the values of the reflection parameters *R*, *IRC* and *MM* did not reveal the histologically confirmed PG loss in a human sample. Although the surface was visually intact in the histological image, the superficial collagen matrix of the sample might have been damaged, because the *URI* value of the PG depleted human sample was of the same order of magnitude as the *URI* values of the mechanically degenerated bovine cartilage samples. Thus, the variation in the ultrasonically determined roughness may be a more characteristic sign of incipient degenerative changes in cartilage than the variation in the specular ultrasound reflection.

The normalized amplitude of the ultrasound reflection from the cartilage surface (*IRC*, *R* and *MM*) depended on the frequency of the ultrasound. The frequency dependence is probably due to different proportions of scattering and specular reflection at the cartilage surface, because dispersion of the speed of sound is minimal in soft tissues [153].

In this thesis, the 50 MHz transducer (table 5.2), which has a beam diameter of 120 μm, best met the requirements for frequency, focusing and size of the beam diameter [23, 24] for evaluating the roughness of a surface of a sample. However, due to the different focusing properties of the ultrasound transducers used in study III, the individual effects of ultrasound frequency and focusing could not be separated.

In study III, it was shown that the size of the spatial sampling step can be increased up to the size of the beam diameter without any significant loss of information. The temporal sampling frequency affected significantly the values of the QUI parameters, but as long as the Nyquist sampling rule [114] was satisfied, the diagnostic power of the ultrasound system was not compromised. This was confirmed by the fact that the *intact* and *degraded* sample groups could always be distinguished.

7.5 Limitations of ultrasonic modeling of articular cartilage

In study IV, the ultrasonic pulse-echo modeling of articular cartilage was conducted. In the model, both the measurement geometry and the structure and composition of the cartilage tissue were simplified considerably.

An obvious limitation of the present model is that it is two-dimensional, and consequently cannot fully represent the real three-dimensional measurement situation. The modeling was limited to two dimensions for practical reasons, because a corresponding 3D Wave 3000 model with a voxel size of $(3.57\ \mu\text{m})^3 \approx 45\ \mu\text{m}^3$ and a transducer-sample distance of 3 mm would have required over 40 GB of random access memory.

Articular cartilage is a highly anisotropic tissue with multiple phases and a fiber matrix structure. In the acoustic model, the assumption of homogeneity and isotropy of the cartilage material was a considerable simplification, but the effects of the sim-

plifications were probably reduced because only the ultrasound reflection from the surface of the cartilage was considered. Furthermore, in the model, the shear ultrasound wave was negligible compared with the longitudinal ultrasound wave. This assumption is justified because the absorption of shear waves in soft tissues is much greater than that of longitudinal waves [41, 94]. This is especially true for cartilage tissue that may contain as much as 80% water.

In the future, adding anisotropy and layers with different compositions would bring the acoustic model of cartilage closer to the real measurement situation. Since osteoarthritic changes are concurrent in cartilage and bone, simultaneous ultrasonic evaluation of cartilage and bone may be diagnostically valuable. Inclusion of subchondral bone in the acoustic model is feasible, because FDTD modeling of bone has been successfully applied earlier [9, 46, 59, 108]. An acoustic model including realistically implemented cartilage and bone might enable more accurate interpretation of high-frequency ultrasound measurements.

CHAPTER VIII

Summary and conclusions

Quantitative ultrasound imaging (QUI) shows significant clinical potential for diagnosis of degenerative cartilage diseases, such as OA. This thesis work continued the investigation and validation of ultrasound methods using experimental and numerical tools. The main conclusions of this thesis are summarized as follows:

1. Complex wavelet transform QUI parameters, the *MM* and the *ED*, provided no additional information about the integrity of articular cartilage compared with the time and frequency domain parameters (*R*, *URI*, *IRC*).

2. The ultrasound roughness parameter *URI*, as well as the reflection parameters *IRC* and *R*, was significantly affected by the angle of incidence of the ultrasound beam. However, in contrast to the reflection parameters, the angular dependence of the *URI* was similar for intact and denegerated cartilage, and thus the diagnostic power was maintained regardless of the angle of incidence up till 7°.

3. In order to evaluate the *URI* reliably, a focused ultrasound transducer must be used. Ultrasound frequency must be greater than 5 MHz; in this thesis it was found that 50 MHz was sufficient. Increasing the spatial step size does not affect the diagnostic power of the QUI parameters as long as the step is smaller than the ultrasound beam diameter at the focus. The limit for the temporal sampling frequency is the Nyquist sampling frequency, above which the diagnostic power of the QUI parameters is preserved.

4. The first ever sample-specific FDTD model for ultrasonic measurements of articular cartilage in a pulse-echo geometry was constructed. The model was successful in reproducing experimentally determined results. It was confirmed that in addition to the roughness of the surface of the cartilage, the values of the material parameters also have a significant impact on the ultrasound reflection. Beyond an angle of incidence of 2° of the ultrasound beam, the increased proportion of scattering (compared with specular reflection) and the decrease of the signal-to-noise ratio caused the *IRC* to become constant.

In conclusion, among the parameters measured in the present studies, the *URI* seems to be the most optimal parameter in detecting the first signs of OA and it is least affected by the angle of incidence of the ultrasound. However, the clinical application of the *URI* imposes major technical demands on the imaging system. The reflection

parameters *R* and *IRC* have the advantage of maintaining their usability with lower ultrasound frequencies than the *URI*. Thus, they might be especially suitable for use with the recently introduced novel minimally invasive ultrasound method, where the condition of articular cartilage and subchondral bone is assessed with an intra-articular ultrasound probe [147].

Although the methods presented in this thesis are not readily applicable for clinical use, they provide valuable guidelines concerning the technical factors affecting the ultrasonic evaluation of the integrity of the articular cartilage and form the basis for further development of clinical ultrasonic applications.

[1] P. S. Addison. *The illustrated wavelet transform handbook*. IOP Publishing Ltd, Bristol, 2002.

[2] R. S. Adler, D. K. Dedrick, T. J. Laing, E. H. Chiang, C. R. Meyer, P. H. Bland, and J. M. Rubin. Quantitative assessment of cartilage surface roughness in osteoarthritis using high frequency ultrasound. *Ultrasound Med Biol*, 18(1):51–8, 1992.

[3] D. H. Agemura, W. D. O'Brien Jr., J. E. Olerud, L. E. Chun, and D. E. Eyre. Ultrasonic propagation properties of articular cartilage at 100 MHz. *J Acoust Soc Am*, 87(4):1786–91, 1990.

[4] R. D. Altman. Overview of osteoarthritis. *Am J Med*, 83(4B):65–9, 1987.

[5] J. M. Anderson-MacKenzie, H. L. Quasnichka, R. L. Starr, E. J. Lewis, E. J. Billingham, and A. J. Bailey. Fundamental subchondral bone changes in spontaneous knee osteoarthritis. *Int J Biochem Cell Biol*, 37:224–236, 2005.

[6] C. G. Armstrong and V. C. Mow. Variations in the intrinsic mechanical properties of human articular cartilage with age, degeneration, and water content. *J Bone Joint Surg Am*, 64(1):88–94, 1982.

[7] G. A. Ateshian. The role of interstitial fluid pressurization in articular cartilage lubrication. *J Biomech*, 42:1163–1176, 2009.

[8] G. A. Ateshian, L. J. Soslowsky, and V. C. Mow. Quantitation of articular surface topography and cartilage thickness in knee joints using stereophotogrammetry. *J Biomech*, 24(8):761–776, 1991.

[9] A. S. Aula, J. Töyräs, M. A. Hakulinen, and J. S. Jurvelin. Effect of bone marrow on acoustic properties of trabecular bone - 3D finite difference modeling study. *Ultrasound Med Biol*, 35(2):308–318, 2009.

[10] M. Aurich, G. R. Squires, A. Reiner, J. A. Mollenhauer, K. E. Kuettner, A. R. Poole, and A. A. Cole. Differential matrix degradation and turnover in early cartilage lesions of human knee and ankle joints. *Arthritis Rheum*, 52(1):112–119, 2005.

[11] A. J. Bailey, J. P. Mansell, T. J. Sims, and X. Banse. Biochemical and mechanical properties of subchondral bone in osteoarthritis. *Biorheology*, 41:349–358, 2004.

[12] F. J. Blanco, R. Guitian, E. Vázquez-Martul, F. J. deToro, and F. Galdo. Osteoarthritis chondrocytes die by apoptosis. *Arthritis Rheum*, 41(2):284–289, 1998.

[13] C. P. Brown, S. W. Hughes, R. W. Crawford, and A. Oloyede. Ultrasound assess-

ment of articular cartilage: analysis of the frequency profile of reflected signals from naturally and artificially degraded samples. *Connect Tissue Res*, 48(6):277–285, 2007.

[14] C. P. Brown, S. W. Hughes, R. W. Crawford, and A. Oloyede. Joint laminate degradation assessed by reflected ultrasound from the cartilage surface and osteochondral junction. *Phys Med Biol*, 53:4123–4135, 2008.

[15] J. A. Buckwalter. Evaluating methods of restoring cartilaginous articular surfaces. *Clin Orthop Relat Res*, (367 Suppl):S224–38, 1999.

[16] J. A. Buckwalter and H. J. Mankin. Articular cartilage: Part I. Tissue design and chondrocyte-matrix interactions. *J Bone Joint Surg Am*, 79-A(4):600–611, 1997.

[17] J. A. Buckwalter and J. Martin. Degenerative joint disease. *Clin Symp*, 47(2):1–32, 1995.

[18] J. A. Buckwalter and J. A. Martin. Osteoarthritis. *Adv Drug Deliv Rev*, 58(2):150–167, 2006.

[19] L. V. Burgin and M. A. Richard. Impact testing to determine the mechanical properties of articular cartilage in isolation and on bone. *J Mater Sci Mater Med*, 19(2):703–711, 2008.

[20] S. Chaffaî, F. Peyrin, S. Nuzzo, R. Porcher, G. Berger, and P. Laugier. Ultrasonic characterization of human cancellous bone using transmission and backscatter measurements: relationships to density and microstructure. *Bone*, 30(1):229–237, 2002.

[21] R. E. Challis and R. I. Kitney. Biomedical signal processing (in four parts). Part 1. Time-domain methods. *Med Biol Eng Comput*, 28(6):509–24, 1990.

[22] J. Charnley. The lubrication of animal joints in relation to surgical reconstruction by arthroplasty. *Ann Rheum Dis*, 19:10–19, 1960.

[23] E. H. Chiang, R. S. Adler, C. R. Meyer, J. M. Rubin, D. K. Dedrick, and T. J. Laing. Quantitative assessment of surface roughness using backscattered ultrasound: the effects of finite surface curvature. *Ultrasound Med Biol*, 20(2):123–135, 1994.

[24] E. H. Chiang, T. J. Laing, C. R. Meyer, J. L. Boes, J. M. Rubin, and R. S. Adler. Ultrasonic characterization of in vitro osteoarthritic articular cartilage with validation by confocal microscopy. *Ultrasound Med Biol*, 23(2):205–213, 1997.

[25] E. Chérin, A. Saïed, P. Laugier, P. Netter, and G. Berger. Evaluation of acoustical parameter sensitivity to age-related and osteoarthritic changes in articular cartilage using 50-MHz ultrasound. *Ultrasound Med Biol*, 24(3):341–354, 1998.

[26] E. Chérin, A. Saïed, B. Pellaumail, D. Loeuille, P. Laugier, P. Gillet, P. Netter, and G. Berger. Assessment of rat articular cartilage maturation using 50-MHz quantitative ultrasonography. *Osteoarthritis Cartilage*, 9:178–186, 2001.

[27] I. Daubechies. *Ten lectures on wavelets*. CNMS-NSF Regional conference series in applied mathematics. Society for Industrial and Applied Mathematics, Philadelphia, 1992.

[28] J. S. Day, J. C. van der Linden, R. A. Bank, M. Ding, I. Hvid, D.R. Sumner, and H. Weinans. Adaptation of subchondral bone in osteoarthritis. *Biorheology*, 41:359–368, 2004.

[29] D. G. Disler, E. Raymond, D. A. May, J. S. Wayne, and T. R. McCauley. Articular cartilage defects: in vitro evaluation of accuracy and interobserver reliability for detection and grading with US. *Radiology*, 215(3):846–851, 2000.

[30] F. G. Donnan. The theory of membrane equilibria. *Chem Rev*, 1:73–90, 1924.

[31] D. J. Dowsett, P. A. Kenny, and R. E. Johnston. *The Physics of Diagnostic Imaging*. Hodder Arnold, London, 2006.

[32] G. N. Duda, A. Haisch, M. Endres, C. Gebert, D. Schroeder, J. E. Hoffmann, and M. Sittinger. Mechanical quality of tissue engineered cartilage: results after 6 and 12 weeks in vivo. *J Biomed Mater Res (Appl Biomater)*, 53:673–677, 2000.

[33] K. R. Erikson, F. J. Fry, and P. J. Joie. Ultrasound in medicine-a review. *IEEE Trans Sonics Ultrason*, SU-21(3):144–170, 1974.

[34] S. C. Faber, F. Eckstein, S. Lukasz, R. Mühlbauer, J. Hohe, K.-H. Englmeier, and M. Reiser. Gender differences in knee joint cartilage thickness, volume and articular surface areas: assessment with quantitative three-dimensional MR imaging. *Skeletal Radiol*, 30:144–150, 2001.

[35] T. C. Fenter, M. J. Naslund, M. B. Shah, M. T. Eaddy, and L. Black. The cost of treating the 10 most prevalent diseases in men 50 years of age or older. *Am J Manag Care*, 12:S90–S98, 2006.

[36] S. Fields and F. Dunn. Correlation of echographic visualizability of tissue with biological composition and physiological state. *J Acoust Soc Am*, 54(3):809–812, 1973.

[37] M. A. Fink and J.-F. Cardoso. Diffraction effects in pulse-echo measurement. *IEEE Trans Sonics Ultrason*, SU-31(4):313–329, 1984.

[38] H. Forster and J. Fisher. The influence of loading time and lubricant on the friction of articular cartilage. *Proc Inst Mech Eng H*, 210(2):109–19, 1996.

[39] H. Forster and J. Fisher. The influence of continuous sliding and subsequent surface wear on the friction of articular cartilage. *Proc Inst Mech Eng H*, 213(4):329–345, 1999.

[40] M. A. Freeman. Is collagen fatigue failure a cause of osteoarthrosis and prosthetic component migration? A hypothesis. *J Orthop Res*, 17(1):3–8, 1999.

[41] L. A. Frizzell, E. L. Carstensen, and J. F: Dyro. Shear properties of mammalian tissues at low megahertz frequencies. *J Acoust Soc Am*, 60(6):1409–1411, 1976.

[42] J. P. Gleghorn, A. R. C. Jones, C. R. Flannery, and L. J. Bonassar. Boundary mode lubrication of articular cartilage by recombinant human lubricin. *J Orthop Res*, 27(6):771–777, 2009.

[43] S.A. Goss and W. D. O'Brien Jr. Direct ultrasonic velocity measurements of mammalian collagen threads. *J Acoust Soc Am*, 65(2):507–511, 1979.

[44] G. Guglielmi and F. de Terlizzi. Quantitative ultrasound in the assessment of osteoporosis. *Eur J Radiol*, 2009.

[45] S. Gupta, G. A. Hawker, A. Laporte, R. Croxford, and P. C. Coyte. The economic burden of disabling hip and knee osteoarthritis (OA) from the perspective of individuals living with this condition. *Rheumatology*, 44:1531–1537, 2005.

[46] G. Haïat, F. Padilla, and P. Laugier. Sensitivity of QUS parameters to controlled variations of bone strength assessed with a cellular model. *IEEE Trans Ultrason Ferroelectr Freq Control*, 55(7):1488–1496, 2008.

[47] M. A. Hakulinen, J. S. Day, J. Töyräs, M. Timonen, H. Kroger, H. Weinans, I. Kiviranta, and J. S. Jurvelin. Prediction of density and mechanical properties of human trabecular bone in vitro by using ultrasound transmission and backscattering measurements at 0.2-6.7 MHz frequency range. *Phys Med Biol*, 50(8):1629–1642, 2005.

[48] F. M. Hall and G. Wyshak. Thickness of articular cartilage in the normal knee. *J*

Bone Joint Surg, 62-A(3):408–413, 1980.

[49] R. A. Harris, D. H. Follett, M. Halliwell, and P. N. Wells. Ultimate limits in ultrasonic imaging resolution. *Ultrasound Med Biol*, 17(6):547–58, 1991.

[50] E. M. Hasler, W. Herzog, J. Z. Wu, W. Muller, and U. Wyss. Articular cartilage biomechanics: theoretical models, material properties, and biosynthetic response. *Crit Rev Biomed Eng*, 27(6):415–88, 1999.

[51] K. Hattori, K. Ikeuchi, Y. Morita, and Y. Takakura. Quantitative ultrasonic assessment for detecting microscopic cartilage damage in osteoarthritis. *Arthritis Res Ther*, 7:R38–R46, 2004.

[52] K. Hattori, K. Mori, T. Habata, Y. Takakura, and K. Ikeuchi. Measurement of the mechanical condition of articular cartilage with an ultrasonic probe: quantitative evaluation using wavelet transformation. *Clin Biomech*, 18:553–557, 2003.

[53] K. Hattori, Y. Takakura, M. Ishimura, T. Habata, K. Uematsu, and K. Ikeuchi. Quantitative arthroscopic ultrasound evaluation of living human cartilage. *Clin Biomech*, 19:213–216, 2004.

[54] K. Hattori, Y. Takakura, M. Ishimura, Y. Tanaka, T. Habata, and K. Ikeuchi. Differential acoustic properties of early cartilage lesions in living human knee and ankle joints. *Arthritis Rheum*, 52(10):3125–3131, 2005.

[55] K. Hattori, Y. Takakura, H. Ohgushi, T. Habata, K. Uematsu, and K. Ikeuchi. Novel ultrasonic evaluation of tissue-engineered cartilage for large osteochondral defects - non-invasive judgment of tissue-engineered cartilage. *J Orthop Res*, 23:1179–1183, 2005.

[56] K. Hattori, Y. Takakura, H. Ohgushi, T. Habata, K. Uematsu, J. Yamauchi, K. Yamashita, T. Fukuchi, M. Sato, and K. Ikeuchi. Quantitative ultrasound can assess the regeneration process of tissue-engineered cartilage using a complex between adherent bone marrow cells and a three-dimensional scaffold. *Arthritis Res Ther*, 7:R552–R559, 2005.

[57] B. K. Hoffmeister, D. P. Johnston, J. A. Janeski, D. A. Keedy, B. W. Steinert, A. M. Viano, and S. C. Kaste. Ultrasonic characterization of human cancellous bone in vitro using three different apparent backscatter parameters in the frequency range 0.6-15.0 MHz. *IEEE Trans Ultrason Ferroelectr Freq Control*, 55(7):1442–1452, 2008.

[58] B. K. Hoffmeister, S. A. Whitten, S. C. Kaste, and J. Y. Rho. Effect of collagen and mineral content on the high-frequency ultrasonic properties of human cancellous bone. *Osteoporos Int*, 13:26–32, 2002.

[59] A. Hosokawa. Development of a numerical cancellous bone model for finite-difference time-domain simulations of ultrasound propagation. *IEEE Trans Ultrason Ferroelectr Freq Control*, 55(6):1219–1233, 2008.

[60] K. Hu, P. Radhakrishnan, R. V. Patel, and J. J. Mao. Regional structural and viscoelastic properties of fibrocartilage upon dynamic nanoindentation of the articular condyle. *J Struct Biol*, 136(1):46–52, 2001.

[61] Y.-P. Huang and Y. P. Zheng. Intravascular ultrasound (IVUS): a potential arthroscopic tool for quantitative assessment of articular cartilage. *Open Biomed Eng J*, 3:13–20, 2009.

[62] B. Jaffré, A. Watrin, D. Loeuille, P. Gillet, P. Netter, P. Laugier, and A. Saïed. Effects of antiinflammatory drugs on arthritic cartilage. *Arthritis Rheum*, 48(6):1594–1601, 2003.

[63] C.-B. James and T.L. Uhl. A review of articular cartilage pathology and the use of glucosamine sulfate. *J Athl Train*, 36(4):413–419, 2001.

[64] G. D. Jay, J. R. Torres, M. L. Warman, M. C. Laderer, and K. S. Breuer. The role of lubricin in the mechanical behavior of synovial fluid. *Proc Natl Acad Sci USA*, 104(15):6194–6199, 2007.

[65] G. A. Joiner, E. R. Bogoch, K. P. Pritzker, M. D. Buschmann, A. Chevrier, and F. S. Foster. High frequency acoustic parameters of human and bovine articular cartilage following experimentally-induced matrix degradation. *Ultrason Imaging*, 23(2):106–116, 2001.

[66] J. P. Jones. Quantitative characterization of tissue using ultrasound. *IEEE Trans Nucl Sci*, NS-27(3):1168–1175, 1980.

[67] D. Joseph, W. Y. Gu, X. G. Mao, W. M. Lai, and V. C. Mow. True density of normal and enzymatically treated bovine articular cartilage. *Trans Orthop Res Soc*, 24:642, 1999.

[68] P. Julkunen, T. Harjula, J. Iivarinen, J. Marjanen, K. Seppänen, T. Närhi, J. Arokoski, M. J. Lammi, P. A. Brama, J. S. Jurvelin, and H. J. Helminen. Biomechanical, biochemical and structural correlations in immature and mature rabbit articular cartilage. *Osteoarthritis Cartilage*, in press, 2009.

[69] J. Jurvelin, T. Kuusela, R. Heikkilä, A. Pelttari, I. Kiviranta, M. Tammi, and H. J. Helminen. Investigation of articular cartilage surface morphology with a semiquantitative scanning electron microscopic method. *Acta Anat*, 116(4):302–311, 1983.

[70] J. P. Karjalainen, J. Töyräs, O. Riekkinen, M. Hakulinen, and J. S. Jurvelin. Ultrasound backscatter imaging provides frequency-dependent infromation on structure, composition and mechanical properties of human trabecular bone. *Ultrasound Med Biol*, 35(8):1376–1384, 2009.

[71] M. A. Karsdal, L. B. Tanko, B. J. Riis, B. C. Sondergard, K. Henriksen, R. D. Altman, P. Qvist, and C. Christiansen. Review: Calsitonin is involved in cartilage homeostasis: Is calcitonin a treatment for OA? *Osteoarthritis Cartilage*, 14:617–624, 2006.

[72] G. E. Kempson, H. Muir, C. Pollard, and M. Tuke. The tensile properties of the cartilage of human femoral condyles related to the content of collagen and glycosaminoglycans. *Biochim Biophys Acta*, 297(2):456–72, 1973.

[73] H. K. Kim, P. S. Babyn, K. A. Harasiewicz, H. K. Gahunia, K. P. Pritzker, and F. S. Foster. Imaging of immature articular cartilage using ultrasound backscatter microscopy at 50 MHz. *J Orthop Res*, 13(6):963–70, 1995.

[74] I. Kiviranta, J. Jurvelin, M. Tammi, A. M. Säämänen, and H. J. Helminen. Microspectrophotometric quantitation of glycosaminoglycans in articular cartilage sections stained with safranin O. *Histochemistry*, 82(3):249–55, 1985.

[75] P. Kiviranta, E. Lammentausta, J. Töyräs, I. Kiviranta, and J. S. Jurvelin. Indentation diagnostics of cartilage degeneration. *Osteoarthritis Cartilage*, 16(7):796–804, 2008.

[76] P. Kiviranta, J. Rieppo, R. K. Korhonen, P. Julkunen, J. Töyräs, and J. S. Jurvelin. Collagen network primarily controls Poisson's ratio of bovine articular cartilage in compression. *J Orthop Res*, 24(4):690–699, 2006.

[77] P. Kiviranta, J. Töyräs, M. T. Nieminen, M S. Laasanen, S. Saarakkala, H. J. Nieminen, M. J. Nissi, and J. S. Jurvelin. Comparison of novel clinically ap-

plicable methodology for sensitive diagnostics of cartilage degeneration. *Eur Cell Mater*, 13:46–55, 2007.

[78] R. U. Kleemann, H. Schell, M. Thompson, D. R. Epari, G. N. Duda, and A. Weiler. Mechanical behavior of articular cartilage after osteochondral autograft transfer in an ovine model. *Am J Sports Med*, 35(4):555–563, 2007.

[79] E. E. Konofagou, T. P. Harrigan, J. Ophir, and T. A. Krouskop. Poroelastography: imaging the poroelastic properties of tissues. *Ultrasound Med Biol*, 27(10):1387–1397, 2001.

[80] R. K. Korhonen, M. Wong, J. Arokoski, R. Lindgren, H. J. Helminen, E. B. Hunziker, and J. S. Jurvelin. Importance of the superficial tissue layer for the indentation stiffness of articular cartilage. *Med Eng Phys*, 24:99–108, 2002.

[81] H. Kuroki, Y. Nakagawa, K. Mori, M. Ohba, T. Suzuki, Y. Mizuno, K. Ando, M. Takenaka, K. Ikeuchi, and T. Nakamura. Acoustic stiffness and change in plug cartilage over time after autologous osteochondral grafting: correlation between ultrasound signal intensity and histological score in a rabbit model. *Arthritis Res Ther*, 6:R492–R504, 2004.

[82] M. S. Laasanen, S. Saarakkala, J. Töyräs, J. Rieppo, and J. S. Jurvelin. Site-specific ultrasound reflection properties and superficial collagen content of bovine knee articular cartilage. *Phys Med Biol*, 50:3221–3233, 2005.

[83] M. S. Laasanen, J. Töyräs, J. Hirvonen, S. Saarakkala, R. K. Korhonen, M. T. Nieminen, I. Kiviranta, and J. S. Jurvelin. Novel mechano-acoustic technique and instrument for diagnosis of cartilage degeneration. *Physiol Meas*, 23(3):491–503, 2002.

[84] M. S. Laasanen, J. Töyräs, R. K. Korhonen, J. Rieppo, S. Saarakkala, M. T. Nieminen, J. Hirvonen, and J. S. Jurvelin. Biomechanical properties of knee articular cartilage. *Biorheology*, 40(1-3):133–140, 2003.

[85] M. S. Laasanen, J. Töyräs, A. Vasara, S. Saarakkala, M. M. Hyttinen, I. Kiviranta, and J. S. Jurvelin. Quantitative ultrasound imaging of spontaneous repair of porcine cartilage. *Osteoarthritis Cartilage*, 14:258–263, 2006.

[86] R. C. Lawrence, D. T. Felson, C. G. Helmick, L. M. Arnold, H. Choi, R. A. Deyo, S. Gabriel, R. Hirsch, M. C. Hochberg, G. G. Hunder, J. M. Jordan, J. N. Katz, H. M. Kremers, and F. Wolfe. Estimates of the prevalence of arthritis and other rheumatic conditions in the United States. *Arthritis Rheum*, 58(1):26–35, 2008.

[87] C. Le Pen, C. Reygrobellet, and I. Gérentes. Financial cost of osteoarthritis in France. the "COART" France study. *Joint Bone Spine*, 72:567–570, 2005.

[88] C.-L. Lee, M.-H. Huang, C.-Y. Chai, C.-H. Chen, J.-Y. Su, and Y.-C. Tien. The validity of in vivo ultrasonographic grading of osteoarthritic femoral condylar cartilage: a comparison with in vitro ultrasonographic and histologic gradings. *Osteoarthritis Cartilage*, 16(3):352–358, 2008.

[89] S. Lees, J. D. Heeley, J. M. Ahern, and M. G. Oravecz. Axial phase velocity in rat tail tendon fibers at 100 MHz by ultrasonic microscopy. *IEEE Trans Sonics Ultrason*, 30(2):85–90, 1983.

[90] S. Leicht and K. Raum. Acoustic impedance changes in cartilage and subchondral bone due to primary arthrosis. *Ultrasonics*, 48(6-7):613–620, 2008.

[91] H. Y. Ling, Y. P. Zheng, and S. G. Patil. Strain dependence of ultrasound speed in bovine articular cartilage under compression in vitro. *Ultrasound Med Biol*, 33(10):1599–1608, 2007.

[92] M. Linzer and S. J. Norton. Ultrasonic tissue characterization. *Annu Rev Biophys Bioeng*, 11:303–329, 1982.

[93] M.-H. Lu, Y. P. Zheng, Q.-H. Huang, C. Ling, Q. Wang, L. Bridal, L. Qin, and A. Mak. Noncontact evaluation of articular cartilage degeneration using a novel ultrasound water jet indentation system. *Ann Biomed Eng*, 37(1):164–175, 2009.

[94] E. L. Madsen, H. J. Sathoff, and J. A. Zagzebski. Ultrasonic shear wave properties of soft tissues and tissuelike materials. *J Acoust Soc Am*, 74(5):1346–1355, 1983.

[95] H. J. Mankin, H. Dorfman, L. Lippiello, and A. Zarins. Biochemical and metabolic abnormalities in articular cartilage from osteo-arthritic human hips. II. Correlation of morphology with biochemical and metabolic data. *J Bone Joint Surg Am*, 53(3):523–537, 1971.

[96] H. J. Mankin and A. Z. Thrasher. Water content and binding in normal and osteoarthritic human cartilage. *J Bone Joint Surg Am*, 57(1):76–80., 1975.

[97] A. Maroudas. Distribution and diffusion of solutes in articular cartilage. *Biophys J*, 10(5):365–379, 1970.

[98] A. Maroudas and M. Venn. Chemical composition and swelling of normal and osteoarthrotic femoral head cartilage. II. Swelling. *Ann Rheum Dis*, 36(5):399–406., 1977.

[99] C. W. Mc Cutchen. The frictional properties of animal joints. *Wear*, 5:1–17, 1962.

[100] T. McAlindon, M. Formica, M. LaValley, M. Lehmer, and K. Kabbara. Effectiveness of glucosamine for symptoms of knee osteoarthritis: results from an intertet-based randomized double-blind controlled trial. *Am J Med*, 117:643–649, 2004.

[101] C. A. McDevitt. Biochemistry of articular cartilage. Nature of proteoglycans and collagen of articular cartilage and their role in ageing and in osteoarthrosis. *Ann Rheum Dis*, 32(4):364–378, 1973.

[102] G. Meachim. Effect of age on the thickness of adult articular cartilage at the shoulder joint. *Ann Rheum Dis*, 30:43–36, 1971.

[103] G. Meachim. Age-related degeneration of patellar articular cartilage. *J Anat*, 134(Pt 2):365–371, 1982.

[104] R. J. Minns, F. S. Steven, and K. Hardinge. Osteoarthrotic articular cartilage lesions of the femoral head observed in the scanning electron microscope. *J Pathol*, 122(2):63–70, 1977.

[105] V. C. Mow, D. C. Fithian, and M. A. Kelly. Fundamentals of articular cartilage and meniscus biomechanics. In J. W. Ewing, editor, *Articular cartilage and knee joint function: basic science and arthroscopy*. Raven Press Ltd., New York, 1990.

[106] S. L. Murphy, D. M. Strasburg, A. K. Lyden, D. M. Smith, J. F. Koliba, D. P. Dadabhoy, and S. M. Wallis. Effects of activity strategy training on pain and physical activity in older adults with knee or hip osteoarthritis: A pilot study. *Arthritis Care & Research*, 59(10):1480–1487, 2008.

[107] S. L. Myers, K. Dines, D. A. Brandt, K. D. Brandt, and M. E. Albrecht. Experimental assessment by high frequency ultrasound of articular cartilage thickness and osteoarthritic changes. *J Rheumatol*, 22(1):109–16, 1995.

[108] Y. Nagatani, K. Mizuno, T. Saeki, M. Matsukawa, T. Sakaguchi, and H. Hosoi. Numerical and experimental study on the wave attenuation in bone - FDTD simulation of ultrasound propagation in cancellous bone. *Ultrasonics*, 48(6-

7):607–612, 2008.

[109] H. J. Nieminen, S. Saarakkala, M. S. Laasanen, J. Hirvonen, J. S. Jurvelin, and J. Töyräs. Ultrasound attenuation in normal and spontaneously degenerated articular cartilage. *Ultrasound Med Biol*, 30(4):493–500, 2004.

[110] H. J. Nieminen, J. Töyräs, M. S. Laasanen, and J. S. Jurvelin. Acoustic properties of articular cartilage under mechanical stress. *Biorheology*, 43:523–535, 2006.

[111] H. J. Nieminen, J. Töyräs, J. Rieppo, M. T. Nieminen, J. Hirvonen, R. Korhonen, and J. S. Jurvelin. Real-time ultrasound analysis of articular cartilage degradation in vitro. *Ultrasound Med Biol*, 28(4):519–525, 2002.

[112] K. Nishitani, Y. Nakagawa, T. Gotoh, M. Kobayashi, and T. Nakamura. Intraoperative acoustic evaluation of living human cartilage of the elbow and knee during mosaicplasty for osteochondritis dissecans of the elbow. *Am J Sports Med*, 36(12):2345–53, 2008.

[113] M. J. Nissi, J. Töyräs, M. S. Laasanen, J. Rieppo, S. Saarakkala, R. Lappalainen, J. S. Jurvelin, and M. T. Nieminen. Proteoglycan and collagen sensitive MRI evaluation of normal and degenerated articular cartilage. *J Orthop Res*, 22:557–564, 2004.

[114] H. Nyquist. Certain topics in telegraph transmission theory. *Transactions of the A.I.E.E.*, pages 617–644, 1928.

[115] S. P. Oakley and M. N. Lassere. A critical appraisal of quantitative arthroscopy as an outcome measure in osteoarthritis of the knee. *Semin Arthritis Rheum*, 33(2):83–105, 2003.

[116] S. P. Oakley, I. Portek, Z. Szomor, A. Turnbull, G. A. C. Murrell, B. W. Kirkham, and M. N. Lassere. Accuracy and reliability of arthroscopic estimates of cartilage lesion size in a plastic knee simulation model. *Arthroscopy*, 19(3):282–289, 2003.

[117] J. Ophir, I. Cespedes, H. Ponnekanti, Y. Yazdi, and X. Li. Elastography: a quantitative method for imaging the elasticity of biological tissues. *Ultrason Imaging*, 13(2):111–34, 1991.

[118] M. Pagnano and G. Westrich. Successful nonoperative management of chronic osteoarthritis pain of the knee: safety and efficacy of retreatment with intraarticular hyaluronans. *Osteoarthritis Cartilage*, 13:751–761, 2005.

[119] K. J. Parker, R. M. Lerner, and R. C. Waag. Attenuation of ultrasound: magnitude and frequency dependence for frequency characterization. *Radiology*, 153:785–788, 1984.

[120] S. G. Patil, Y. P. Zheng, J. Y. Wu, and J. Shi. Measurement of depth-dependence and anisotropy of ultrasound speed of bovine articular cartilage in vitro. *Ultrasound Med Biol*, 30(7):953–963, 2004.

[121] P. C. Pedersen and A. Grebe. Application of time delay spectrometry for rough surfae characterization. *Ultrasonics*, 39:101–108, 2001.

[122] B. Pellaumail, D. Loeuille, A. Watrin, P. Netter, G. Berger, and A. Saïed. Correlation of high frequency ultrasound backscatter with cartilage matrix constituents. *IEEE Ultrasonics Symposium*, pages 1463–1466, 1998.

[123] B. Pellaumail, A. Watrin, D. Loeuille, P. Netter, G. Berger, P. Laugier, and A. Saïed. Effect of articular cartilage proteoglycan depletion on high frequency ultrasound backscatter. *Osteoarthritis Cartilage*, 10(7):535–541, 2002.

[124] J. Pohlhammer and W. D. O'Brien Jr. Dependence of the ultrasonic scatter

coefficient on collagen concentration in mammalian tissues. *J Acoust Soc Am*, 69(1):283–5, 1981.

[125] C.-J. Qu, H. M. Karjalainen, H. J. Helminen, and M. J. Lammi. The lack of effect of glucosamine sulphate on aggrecan mRNA expression and 35S-sulphate incorporation in bovine promary chondrocytes. *Biochim Biophys Acta*, pages 453–459, 2006.

[126] P. Qvist, A.-C. Bay-Jensen, C. Christiansen, E. B. Dam, P. Pastoureau, and M. A. Karsdal. The disease modifying osteoarthritis drug (DMOAD): Is it in the horizon? *Pharmacol Res*, 58:1–7, 2008.

[127] E. L. Radin, I. L. Paul, and M. J. Tolkoff. Subchondral bone changes in patients with early degenerative joint disease. *Arthritis Rheum*, 13(4):400–5, 1970.

[128] K. Raum and Jr. O'Brien, W. D. Pulse-echo filed distribution measurement technique for high-frequency ultrasound sources. *IEEE Trans Ultrason Ferroelectr Freq Control*, 44(4):810–815, 1997.

[129] J. Rieppo, J. Töyräs, M. T. Nieminen, V. Kovanen, M. M. Hyttinen, R. K. Korhonen, J. S. Jurvelin, and H. J. Helminen. Structure-function relationships in enzymatically modified articular cartilage. *Cells Tissues Organs*, 175(3):121–32, 2003.

[130] J. Rothfuss, W. Mau, H. Zeidler, and M. H. Brenner. Socioeconomic evaluation of rheumatoid arthritis and osteoarthritis: a literature review. *Semin Arthritis Rheum*, 26(5):771–779, 1997.

[131] S. Saarakkala, R. K. Korhonen, M. Laasanen, J. Töyräs, J. Rieppo, and J. S. Jurvelin. Mechano-acoustic determination of Young's modulus of articular cartilage. *Biorheology*, 41:167–179, 2004.

[132] S. Saarakkala, M. S. Laasanen, J. S. Jurvelin, K. Törrönen, M. J. Lammi, R. Lappalainen, and J. Töyräs. Ultrasound indentation of normal and spontaneously degenerated bovine articular cartilage. *Osteoarthritis Cartilage*, 11:697–705, 2003.

[133] S. Saarakkala, M S. Laasanen, J. S. Jurvelin, and J. Töyräs. Quantitative ultrasound imaging detects degenerative changes in articular cartilage surface and subchondral bone. *Phys Med Biol*, 51(20):5333–5346, 2006.

[134] A. Saïed, E. Chérin, H. Gaucher, P. Laugier, P. Gillet, J. Floquet, P. Netter, and G. Berger. Assessment of articular cartilage and subchondral bone: subtle and progressive changes in experimental osteoarthritis using 50 MHz echography in vitro. *J Bone Miner Res*, 12(9):1378–1386, 1997.

[135] D. A. Senzig, F. K. Forster, and J. E. Olerud. Ultrasonic attenuation in articular cartilage. *J Acoust Soc Am*, 92(2):676–681, 1992.

[136] K. Shigematsu, K. Hattori, Y. Kobata, K. Kawamura, H. Yajima, and Y. Takakura. A pilot feasibility study for ultrasound evaluation of living human wrist cartilage: site-specific differences in acoustic properties. *J Hand Surg*, 34A:34–39, 2009.

[137] M. P. Spriet, C. A. Girard, F. S. Foster, K. A. Harasiewicz, D. W. Holdsworth, and S. Laverty. Validation of a 40 MHz B-scan ultrasound biomicroscope for the evaluation of osteoarthritis lesions in an animal model. *Osteoarthritis Cartilage*, 13:171–179, 2005.

[138] G. R. Squires, S. Okouneff, M. Ionescu, and A. R. Poole. The pathobiology of focal lesion development in aging human articular cartilage and molecular matrix changes characteristic of osteoarthritis. *Arthritis Rheum*, 48(5):1261–1270, 2003.

[139] R. A. Stockwell. The interrelationship of cell density and cartilage thickness in mammalian articular cartilage. *J Anat*, 109(3):411–421, 1971.

[140] J.-K. F. Suh, I. Youn, and F. H. Fu. An in situ calibration of an ultrasound transducer: a potential application for an ultrasonic indentation test of articular cartilage. *J Biomech*, 34(10):1347–1353, 2001.

[141] P. D. Thorne and N. G. Pace. Acoustic studies of broadband scattering from a model rough surface. *J Acoust Soc Am*, 75(1):133–144, 1984.

[142] J. Töyräs, R. K. Korhonen, T. Voutilainen, J. S. Jurvelin, and R. Lappalainen. Improvement of arthroscopic cartilage stiffness probe using amorphous diamond coating. *J Biomed Mater Res B Appl Biomater*, 73B(1):15–22, 2005.

[143] J. Töyräs, M. S. Laasanen, S. Saarakkala, M. J. Lammi, J. Rieppo, J. Kurkijärvi, R. Lappalainen, and J. S. Jurvelin. Speed of sound in normal and degenerated bovine articular cartilage. *Ultrasound Med Biol*, 29(3):447–454, 2003.

[144] J. Töyräs, J. Rieppo, M. T. Nieminen, H. J. Helminen, and J. S. Jurvelin. Characterization of enzymatically induced degradation of articular cartilage using high frequency ultrasound. *Phys Med Biol*, 44(11):2723–2733, 1999.

[145] A. I. Vasara, M. M. Hyttinen, M. J. Lammi, P. E.. Lammi, T.K. Långsjö, A. Lindahl, L. Peterson, M. Kellomäki, Y. T. Konttinen, H. J. Helminen, and I. Kiviranta. Subchondral bone reaction associated with chondral defect and attempted cartilage repair in goats. *Calcif Tissue Int*, 74:107–114, 2004.

[146] N. Verzijl, J. DeGroot, R. A. Bank, M. T. Bayliss, J. W. J. Bijlsma, F. P. J. G. Lafeber, A. Maroudas, and J. M. TeKoppele. Age-related accumulation of the advanced glycation endproduct pentosidine in human articular cartilage aggrecan: the use of pentosidine levels as a quantitative measure of protein turnover. *Matrix Biol*, 20:409–417, 2001.

[147] T. Virén, S. Saarakkala, E. Kaleva, H. J. Nieminen, J. S. Jurvelin, and J. Töyräs. Minimally invasive ultrasound method for intra-articular diagnostics of cartilage degeneration. *Ultrasound Med Biol*, 35(9):1546–1554, 2009.

[148] Q. Wang, Y.-P. Zheng, L. Qin, Q.-H. Huang, W.-L. Lam, G. Leung, X. Guo, and H.-B. Lu. Real-time ultrasonic assessment of progressive proteoglycan depletion in articular cartilage. *Ultrasound Med Biol*, 34(7):1085–1092, 2008.

[149] J. S. Wayne, K. A. Kraft, K. J. Shields, C. Yin, J. R. Owen, and D. G. Disler. MR imaging of normal and matrix-depleted cartilage: correlation with biomechanical function and biochemical composition. *Radiology*, 228(2):493–499, 2003.

[150] C. Weiss and S. Mirow. An ultrastructural study of osteoarthritic changes in the articular cartilage of human knees. *J Bone Joint Surg Am*, 54(5):954–72, 1972.

[151] P. N. T. Wells. *Physical principles of ultrasonic diagnosis*, volume 1 of *Medical physics*. Academic Press Inc., New York, 1969.

[152] P. N. T. Wells. Review: absorption and dispersion of ultrasound in biological tissue. *Ultrasound Med Biol*, 1(4):369–76, 1975.

[153] P. N. T. Wells. *Biomedical ultrasonics*. Medical physics. Academic Press Inc., New York, 1977.

[154] J. E. Wilhjelm, P. C. Pedersen, and S. M. Jacobsen. The influence of roughness, angle, range, and transducer type on the echo signal from planar interfaces. *IEEE Trans Ultrason Ferroelectr Freq Control*, 48(2):511–521, 2001.

[155] S. Yongchen, D. Yanwu, T. Jie, and T. Zhensheng. Ultrasonic propagation parameters in human tissues. *Proceedings of Ultrasonics Symposium*, 1986.

[156] I. Youn, F. H. Fu, and J.-K. Suh. Determination of the mechanical properties of articular cartilage using a high-frequency ultrasonic indentation technique. *Trans Orthop Res Soc*, 23:162, 1999.

[157] Y. P. Zheng and Y. P. Huang. More intrinsic parameters should be used in assessing degeneration of articular cartilage with quantitative ultrasound. *Arthritis Res Ther*, 10, 2008.

[158] Y. P. Zheng, M.-H. Lu, and Q. Wang. Ultrasound elastomicroscopy using water jet and osmosis loading: potentials for assessment for articular cartilage. *Ultrasonics*, 44:e203–e209, 2006.

[159] Y. P. Zheng and A. F. Mak. An ultrasound indentation system for biomechanical properties assessment of soft tissues in-vivo. *IEEE Trans Biomed Eng*, 43(9):912–8, 1996.

Kuopio University Publications C. Natural and Environmental Sciences

C 238. Pinto, Delia M. Ozonolysis of constitutively-emitted and herbivory-induced volatile organic compounds (VOCs) from plants: consequences in multitrophic interactions.
2008. 110 p. Acad. Diss.

C 239. Berberat neé Kurkijärvi, Jatta. Quantitative magnetic resonance imaging of native and repaired articular cartilage: an experimental and clinical approach.
2008. 90 p. Acad. Diss.

C 240. Soininen, Pasi. Quantitative ^{1}H NMR spectroscopy: chemical and biological applicatons.
2008. 128 p. Acad. Diss.

C 241. Klemola, Kaisa. Cytotoxicity and spermatozoa motility inhibition resulting from reactive dyes and dyed fabrics.
2008. 67 p. Acad. Diss.

C 242. Pyykönen, Teija. Environmental factors and reproduction in farmed blue fox (Vulpes lagopus) vixens.
2008. 78 p. Acad. Diss.

C 243. Savolainen, Tuomo. Modulaarinen, adaptiivinen impedanssitomografialaitteisto.
2008. 188 p. Acad. Diss.

C 244. Riekkinen, Ossi. Development and application of ultrasound backscatter methods for the diagnostics of trabecular bone.
2008. 79 p. Acad. Diss.

C 245. Autio, Elena. Loose housing of horses in a cold climate: effects on behaviour, nutrition, growth and cold resistance.
2008. 76 p. Acad. Diss.

C 246. Saramäki, Anna. Regulation of the p21 (CDKNIA) gene at the chromatin level by 1 alfa,25-dihydroxyvitamin D3.
2008. 100 p. Acad. Diss.

C 247. Tiiva, Päivi. Isoprene emission from northern ecosystems under climate change.
2008. 98 p. Acad. Diss.

C 248. Himanen, Sari J. Climate change and genetically modified insecticidal plants: plant-herbivore interactions and secondary chemistry of Bt Cryl Ac-Toxin producing oilseed rape (Brassica napus L.) under elevated CO2 or O3.
2008. 42 p. Acad. Diss.

C 249. Silvennoinen, Hanna. Nitrogen and greenhouse gas dynamics in rivers and estuaries of theBothnian Bay (Northern Baltic Sea).
2008. 98 p. Acad. Diss.

C 250. Degenhardt, Tatjana. An integrated view of PPAR-dependent transcription.
2009. 120 p. Acad. Diss.

C 251. Häikiö, Elina. Clonal differences of aspen (Populus spp.) in responses to elevated ozone and soil nitrogen.
2009. 49 p. Acad. Diss.

C 252. Hassinen, Viivi H. Search for metal-responsive genes in plants: putative roles in metal tolerance of accumulation.
2009. 84 p. Acad. Diss.